generative diseases, these observations suggest that Dorfin may have a significant role in the quality control system in the cell. The present study was designed to obtain further clues for the pathophysiological roles of Dorfin. For this purpose, we screened Dorfin-associated proteins using high performance liquid chromatography coupled to electrospray tandem mass spectrometry (LC-MS/MS). The results showed that Valosin-containing protein (VCP), also called p97 or Cdc48 homologue, obtained from the screening, physically and functionally interacted with Dorfin. Furthermore, both Dorfin and VCP proteins colocalized in aggresomes of the cultured cells and in UBIs in various neurodegenerative diseases.

MATERIALS AND METHODS

Plasmids and Antibodies—pCMV2/FLAG-Dorfin vector (FLAG-Dorfin^{WT}) was prepared by PCR using the appropriate design of PCR primers with restriction sites (ClaI and KpnI). The PCR product was digested and inserted into the ClaI-KpnI site in pCMV2 vector (Sigma). pEGFP-Dorfin (GFP-Dorfin), pCMX-VCP^{Wt} (VCP^{Wt}), and pCMX-VCP^{K524A} (VCP^{K524A}) vectors were described previously (5, 11). pcDNA/HA-VCP^{Wt} (HA-VCP^{Wt}) and pcDNA/HA-VCP^{K524A} (HA-VCP^{K524A}) were subcloned from pCMX-VCP^{Wt} and pCMX-VCP^{K524A}, respectively, into pcDNA3.1 vectors (Invitrogen). The HA tag was introduced at the N terminus of VCP. pcDNA3.1/FLAG-Parkin (FLAG-Parkin) was generated by PCR using the appropriate design of PCR primers with restriction sites (EcoRI and NotI) from pcDNA3.1/Myc-Parkin (12). The FLAG tag was introduced at the N terminus of Parkin. To establish the RING mutant plasmid of Dorfin (FLAG-Dorfin$^{C132S/C135S}$), point mutations for Cys at positions 132 and 135 to Ser were generated by PCR-based site-directed mutagenesis using a QuikChange™ site-directed mutagenesis kit (Stratagene, La Jolla, CA). pcDNA3.1/HA-Ub (HA-Ub), pcDNA3.1/Myc-SOD1^{WT} (SOD1^{WT}-Myc), pcDNA3.1/Myc-SOD1^{G93A} (SOD1^{G93A}-Myc), and pcDNA3.1/Myc-SOD1^{G85R} (SOD1^{G85R}-Myc) were described previously (13, 14). Polyclonal anti-Dorfin (Dorfin-30 and Dorfin-41) and monoclonal anti-VCP antibodies were used as in previous reports (5, 15). The following antibodies were used in this study: monoclonal anti-FLAG antibody (M2; Sigma), monoclonal anti-Myc antibody (9E10; Santa Cruz Biotechnology, Santa Cruz, CA), monoclonal anti-HA antibody (12CA5; Roche Applied Science), polyclonal anti-maltose-binding protein (MBP) antibody (New England BioLabs, Beverly, MA), polyclonal anti-Parkin (Cell Signaling, Beverly, MA), and polyclonal anti-SOD1 (SOD-100; Stressgen, San Diego, CA).

Cell Culture and Transfection—All media and reagents for cell culture were purchased from Invitrogen. HEK293 cells were grown in Dulbecco's modified Eagle's medium containing 10% fetal calf serum, 5 units/ml penicillin, and 50 μg/ml streptomycin. HEK293 cells at subconfluence were transfected with the indicated plasmids using FuGENE6 reagent (Roche Applied Science). To inhibit cellular proteasome activity, cells were treated with 1 μM MG132 (benzyloxycarbonyl-Leu-Leu-Leu-al; Sigma) for 16 h after overnight post-transfection. Cells were analyzed at 24–48 h after transfection.

Protein Identification by LC-MS/MS Analysis—FLAG-Dorfin^{WT} was expressed in HEK293 cells (semiconfluent in a 10-cm dish) and then immunoprecipitated by anti-FLAG antibody. The immunoprecipitates were eluted with a FLAG peptide and then digested with Lys-C endopeptidase (*Achromobacter* protease I). The resulting peptides were analyzed using a nanoscale LC-MS/MS system as described previously (16). The peptide mixture was applied to a Mightysil-PR-18 (1-μm particle, Kanto Chemical Corp., Tokyo) column (45 × 0.150 mm ID) and separated using a 0–40% gradient of acetonitrile containing 0.1% formic acid over 30 min at a flow rate of 50 nl/min. Eluted peptides were sprayed directly into a quadrupole time-of-flight hybrid mass spectrometer (Q-Tof *Ultima*; Micromass, Manchester, UK). MS and MS/MS spectra were obtained in data-dependent mode. Up to four precursor ions above an intensity threshold of 10 cps were selected for MS/MS analysis from each survey scan. All MS/MS spectra were searched against protein sequences of Swiss Prot and RefSeq (NCBI) using batch processes of the Mascot software package (Matrix Science, London, UK). The criteria for match acceptance were the following: 1) when the match score was 10 over each threshold, identification was accepted without further consideration; 2) when the difference of score and threshold was lower than 10 or when proteins were identified based on a single matched MS/MS spectrum, we manually confirmed the raw data prior to acceptance; 3) peptides assigned by less than three y series ions and peptides with +4 charge state were all eliminated regardless of their scores.

Recombinant Proteins and Pull-down Assay—We used pMALp2 (New England BioLabs) and pMALp2T (Factor Xa cleavage site of pMALp2 was replaced with a thrombin recognition site) to express fusion proteins with MBP. To produce the full-length (residues 1–838) Dorfin (MBP-Dorfin^{full}), N-terminal (residues 1–367) Dorfin (MBP-Dorfin^{N}), and C-terminal (residues 368–838) Dorfin (MBP-Dorfin^{C}), the PCR fragments were amplified from pcDNA4/HisMax-Dorfin (4) by using the appropriate PCR primers with restriction sites (FbaI and HindIII) and then ligated into pMAL-p2 vectors. To produce the MBP-Parkin protein, full-length *PARKIN* cDNA was inserted into the EcoRI-NotI sites of pMALp2T. All of the MBP-tagged recombinant proteins were purified from *Escherichia coli* BL21-codon-plus. The detail of the purification method of MBP-tagged proteins was described previously (17). Recombinant GST fusion VCP^{WT} and VCP^{K524A} proteins were also generated from *E. coli* lysate and purified with glutathione-Sepharose. Recombinant His-VCP^{WT} and His-VCP^{K524A} proteins were purified from insect cells using baculovirus. The detail of purification of these recombinant VCP proteins was described previously (15). Binding experiments were performed with proteins carrying different tags. His- or GST-VCP were mixed with MBP fusion proteins: MBP-Dorfin^{full}, -Dorfin^{N}, -Dorfin^{C}, -Parkin, and -mock. His-VCP and GST-VCP proteins were precipitated by Ni^{2+}-nitrilotriacetic acid-agarose (Qiagen, Valencia, CA), and glutathione-Sepharose (Amersham Biosciences), respectively. Binding was performed with 1–3 μg of each protein in 300 μl of binding buffer (50 mM Tris-HCl, pH 7.5, 100 mM NaCl, 5 mM $MgCl_2$, 10% glycerol, 0.5 mg/ml bovine serum albumin, 1 mM dithiothreitol) for 1 h at 4 °C. Then 15 μl of beads were added and incubated for 30 min. The beads were washed by binding buffer three times and eluted with sample buffer and analyzed by SDS-PAGE followed by Western blotting using specific antibodies.

Glycerol Gradient Centrifugation—Cultured cells or mouse tissues were homogenized in 1 ml of PBS with protease inhibitor (Complete Mini; Roche Applied Science). Supernatants (1 mg of protein for cultured cells, 5 mg of protein for mouse tissues, and 0.1 mg of recombinant His-VCP protein) were used as the samples after 10,000 × *g* centrifugation for 20 min. The samples (1.0 ml) were loaded on top of a 34-ml linear gradient of glycerol (10–40%) prepared in 25 mM Tris-HCl buffer, pH 7.5, containing 1 mM dithiothreitol in 40 PA centrifuge tubes (Hitachi, Tokyo), and centrifuged at 4 °C and 80,000 × *g* for 22 h using a Himac CP100α centrifuge system (Hitachi). Thirty fractions were collected from the top of the tubes. Two hundred μl of each fraction was precipitated with acetone, and the remaining pellet was lysed with 50 μl of sample buffer and then used for SDS-PAGE followed by Western blotting.

Immunological Analysis—Cells (4 × 10^5 in a 6-cm dish) were lysed with 500 μl of lysis buffer (50 mM Tris-HCl, 150 mM NaCl, 1% Nonidet P-40, and 1 mM EDTA) with protease inhibitor mixture (Complete Mini) 24–48 h after transfection. The lysate was then centrifuged at 10,000 × *g* for 10 min at 4 °C to remove debris. A 10% volume of the supernatants was used as the "lysate" for SDS-PAGE. When immunoprecipitated, the supernatants were precleared with protein A-Sepharose (Amersham Biosciences), and specific antibodies, anti-FLAG (M2), anti-Myc (9E10), or anti-Dorfin (Dorfin-30) were then added and then incubated at 4 °C with rotation. Immune complexes were then incubated with protein A-Sepharose for 3 h, collected by centrifugation, and washed four times with the lysis buffer. For protein analysis, immune complexes were dissociated by heating in SDS-PAGE sample buffer and loaded onto SDS-PAGE. The samples were separated by SDS-PAGE (12% gel or 4–12% gradient gel) and transferred onto a polyvinylidene difluoride membrane. Finally, Western blotting was performed with specific antibodies.

Immunohistochemistry—HEK293 cells grown on glass coverslips were fixed in 4% paraformaldehyde in PBS for 15 min. Then the cells were blocked for 30 min with 5% (v/v) normal goat serum in PBS, incubated for 1 h at 37 °C with anti-HA antibody (12CA5), washed with PBS, and incubated for 30 min with Alexa 496-nm anti-mouse antibodies (Molecular Probes, Inc., Eugene, OR). The coverslips were washed and mounted on slides. Fluorescence images were obtained using a fluorescence microscope (DMIRE2; Leica, Bannockburn, IL) equipped with a cooled charge-coupled device camera (CTR MIC; Leica). Pictures were taken using Leica Qfluoro software.

Pathological Studies—Pathological studies were carried out on 10% formalin-fixed, paraffin-embedded spinal cords and brain stems filed in the Department of Neurology, Nagoya University Graduate School of Medicine. The specimens were obtained at autopsy from three sporadic cases of ALS and four sporadic PD patients. The spinal cord and brain stem specimens of these ALS and PD cases were immunohistochemically stained with antibodies against Dorfin (Dorfin-41) and VCP. Dou-

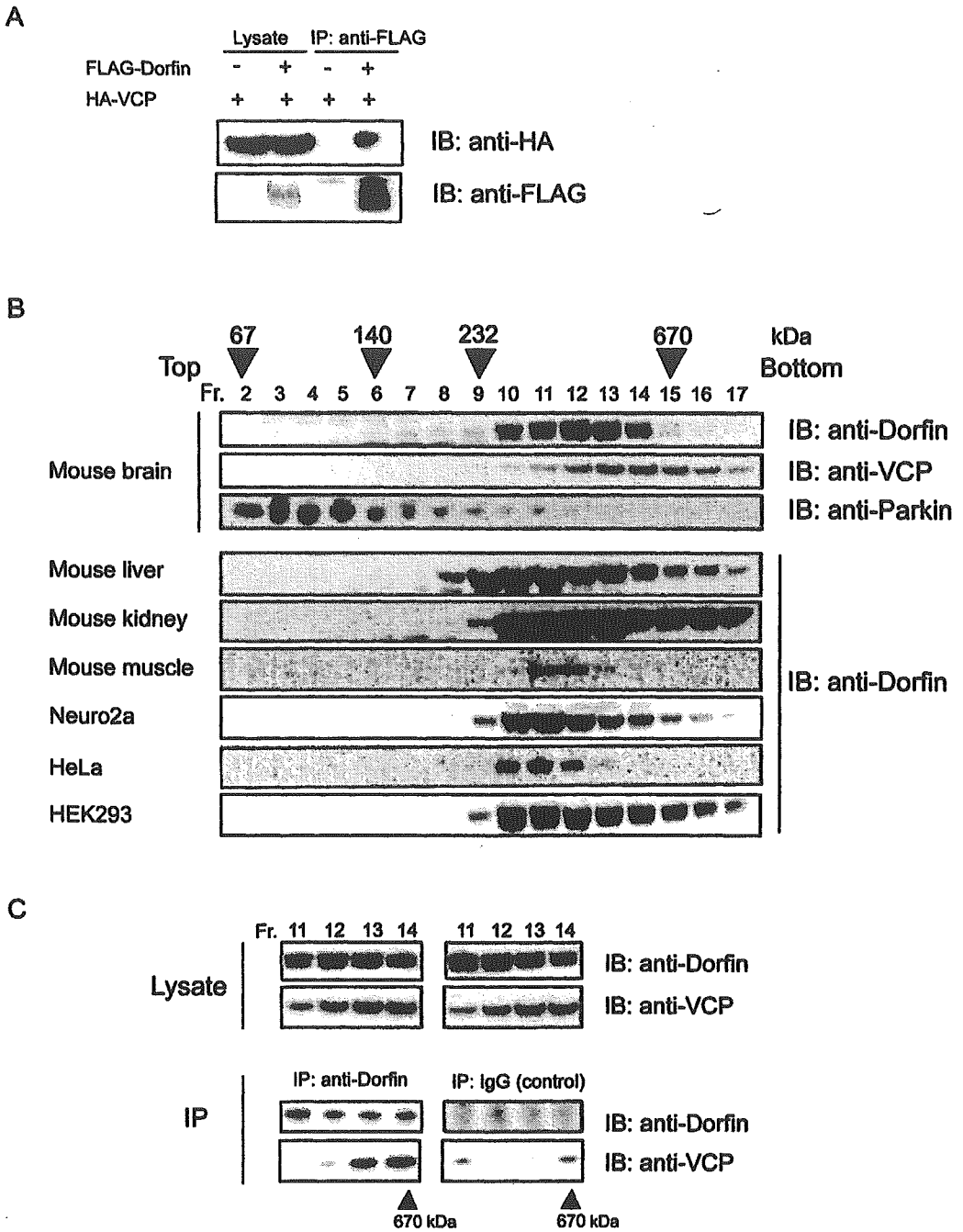

FIG. 1. ***In vivo* interaction between Dorfin and VCP.** *A*, FLAG-Dorfin and HA-VCP are co-expressed in HEK293 cells. FLAG-mock vector was used as a negative control. The amounts of HA-VCP in 10% of the lysate used are shown (*Lysate*); the rest was subjected to immunoprecipitation (*IP*) with anti-FLAG (M2) antibody. Following immunoblotting (*IB*) with anti-HA (12CA5) antibody revealed that HA-VCP was co-immunoprecipitated with FLAG-Dorfin. *B*, 5 mg of protein of various mouse tissues (brain, liver, kidney, and muscle) and 1 mg of protein of cultured cells (HEK293, HeLa, and Neuro2a) were each homogenized in 1 ml of PBS. Supernatants were fractionated by 10–40% glycerol gradient centrifugation followed by separation into 30 fractions using a fraction collector. Immunoblotting using anti-Dorfin, anti-VCP, and anti-Parkin antibodies was performed on the fractions (*Fr.*), including fractions 2–17. Endogenous Dorfin was co-sedimented with VCP in the fractions with a molecular mass of around 400–600 kDa. The positions of co-migrated molecular mass markers are indicated *above* the *panels*. *C*, immunoprecipitation with polyclonal anti-Dorfin antibody (anti-Dorfin-30) was performed on fractions 11–14 collected by glycerol gradient centrifugation analysis, where endogenous Dorfin was seen in *B*. As a negative control, immunoprecipitation with nonimmune rabbit IgG was used on the same fractions.

ble staining of identical sections was performed as described previously (7). In immunofluorescence microscopy, Alexa-488- and Alexa-546-conjugated secondary antibodies (Molecular Probes) were used. All human and animal studies described in this report were approved by the appropriate Ethics Review Committees of the Nagoya University Graduate School of Medicine.

RESULTS

Identification of Dorfin-associated Protein in the Cells—In an effort to identify protein(s) that physically interacts with Dorfin in the cells, FLAG-Dorfin was expressed in HEK293 cells and then immunoprecipitated by anti-FLAG antibody. The immunoprecipitates were eluted with a FLAG peptide and then digested with Lys-C endopeptidase (*Achromobacter* protease I), and the cleaved fragments were directly analyzed using a highly sensitive "direct nanoflow LC-MS/MS" system as described under "Materials and Methods." Following data base search, a total of 13 peptides were assigned to MS/MS spectra obtained from the LC-MS/MS analyses for the FLAG-Dorfin-

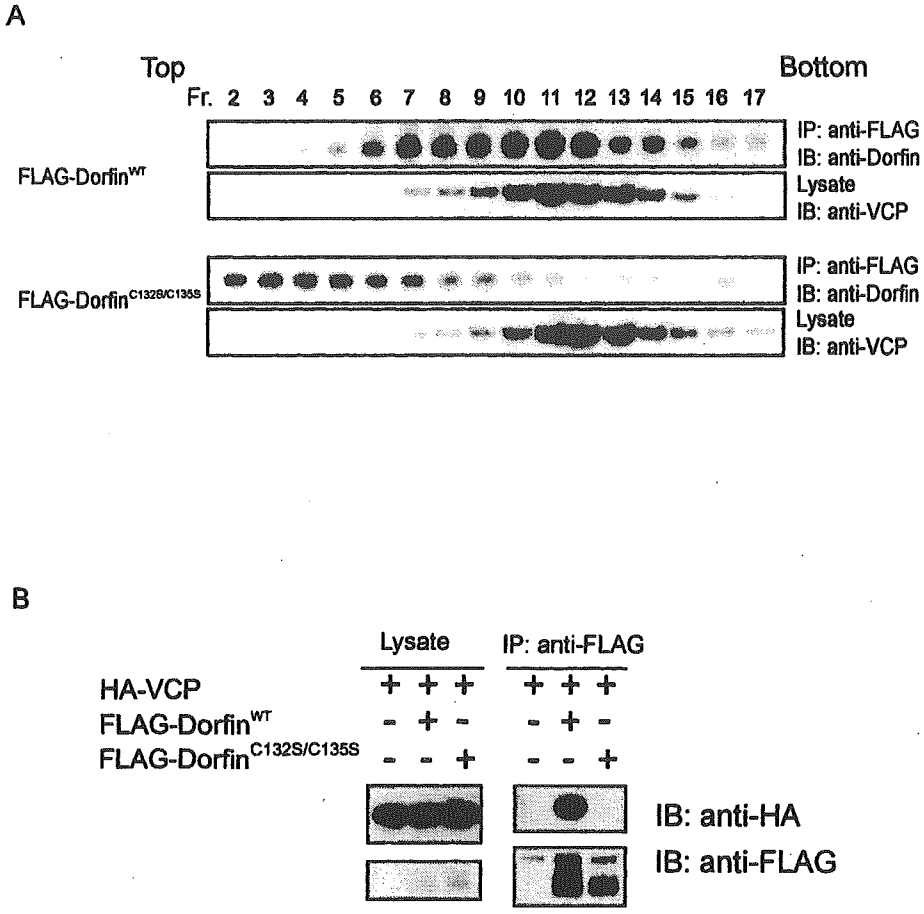

FIG. 2. **Loss of physical interaction between Dorfin$^{C132S/C135S}$ and VCP.** *A*, transfected Dorfin^{WT}, but not Dorfin$^{C132S/C135S}$ (*Dorfin$^{C132S-C135S}$*), forms a high M_r complex. Lysate of HEK293 cells overexpressed with FLAG-Dorfin^{WT} or FLAG-Dorfin$^{C132S/C135S}$ was fractionated by 10–40% glycerol gradient centrifugation. The selected fractions (*Fr.*), fractions 2–17, were subjected to immunoprecipitation (*IP*) using anti-FLAG (M2) antibody. Immunoblotting (*IB*) with anti-Dorfin antibody revealed that exogenous FLAG-Dorfin^{WT} formed a high molecular weight complex, whose peak was at fraction 11, whereas FLAG-Dorfin$^{C132S/C135S}$ migrated in fractions of smaller M_r (around fraction 7). Ten percent of the fractionated samples were shown as "lysate." *B*, Dorfin^{WT} can interact with VCP, but Dorfin$^{C132S/C135S}$ cannot. FLAG-Dorfin^{WT} or FLAG-Dorfin$^{C132S/C135S}$ and HA-VCP were co-expressed in HEK293 cells. FLAG-mock vector was used as a negative control. The amounts of HA-VCP in 10% of the lysate used are shown (*Lysate*); the rest was subjected to immunoprecipitation with anti-FLAG (M2) antibody. Following immunoblotting with anti-HA (12CA5) antibody revealed that HA-VCP was co-immunoprecipitated with FLAG-Dorfin^{WT} but not with FLAG-Dorfin$^{C132S/C135S}$.

associated complexes. These peptide data identified nine proteins as candidates for Dorfin-associated proteins. One of these identified proteins was VCP that has been proposed to have multiple functions, such as membrane fusion or endoplasmic reticulum-associated degradation (ERAD) (18–22). In the next step, we examined the relationship between Dorfin and VCP, because the latter has been reported to be linked to various aspects of neurodegeneration (15).

Dorfin Interacts with VCP in Vivo—To verify the interaction between Dorfin and VCP, FLAG-Dorfin and HA-VCP were transiently overexpressed in HEK 293 cells. Immunological analyses revealed that HA-VCP was co-immunoprecipitated with FLAG-Dorfin but not with FLAG-mock (Fig. 1*A*), confirming their physical interactions in the cells. To determine whether endogenous Dorfin forms a complex, the lysate from mouse brain homogenate was fractioned by glycerol density gradient centrifugation. Each fraction was immunoblotted with anti-Dorfin antibody. The majority of endogenous Dorfin was co-sedimented with VCP around a size of 400–600 kDa, although endogenous Parkin, which is another RING-IBR type E3 ligase (12), existed in the fractions of much lighter molecular weight (M_r) (Fig. 1*B*, *top panels*). Moreover, Dorfin was sedimented in the fractions of 400–600 kDa in other tissues, such as the liver, kidney, and muscle of mouse, and various cultured cells including Neuro2a, HeLa, and HEK293 cells (Fig. 1*B*, *bottom panels*). To determine whether endogenous Dorfin interacts with VCP, immunoprecipitation using polyclonal anti-Dorfin antibody (Dorfin-30) was performed on the fractions shown in Fig. 1*B*, *top panels*. Endogenous VCP was co-immunoprecipitated with endogenous Dorfin in the fractions of high M_r (fractions (*Fr.*) 13 and 14). No apparent band was observed when precipitated with rabbit IgG (Fig. 1*C*).

Mutations of RING Finger Domain of Dorfin Results in Loss of Dorfin-VCP Interactions—Next, we examined whether transfected Dorfin (FLAG-Dorfin^{WT}) and its RING mutant (FLAG-Dorfin$^{C132S/C135S}$), in which the two Cys residues at positions 132 and 135 within the RING finger domain were substituted for Ser residues, form a complex. The results showed overexpression of FLAG-Dorfin^{WT} in high molecular fractions (*Fr.* in Fig. 2), whose peak was between fractions 10 and 12, whereas overexpressed FLAG-Dorfin$^{C132S/C135S}$ did not consist of high molecular weight complex. Overexpression of FLAG-Dorfin^{WT} or FLAG-Dorfin$^{C132S/C135S}$ did not change the sedimentation pattern of VCP (Fig. 2*A*). Furthermore, immunoprecipitation analysis showed that FLAG-Dorfin^{WT}, but not FLAG-Dorfin$^{C132S/C135S}$, could interact with HA-VCP in HEK293 cells (Fig. 2*B*).

Dorfin Interacts with VCP in Vitro—To confirm the direct

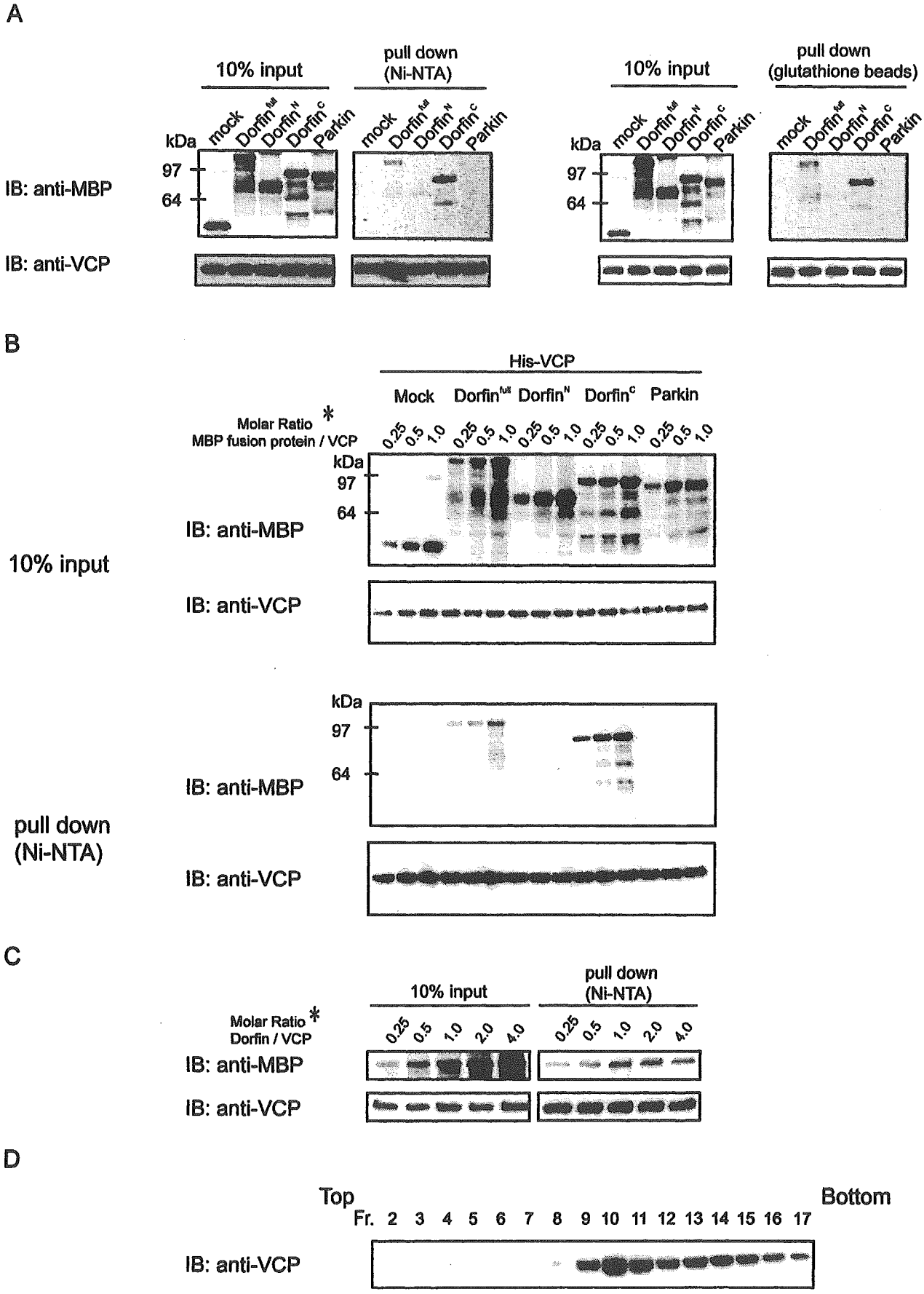

FIG. 3. ***In vitro* interaction between Dorfin and VCP.** *A*, recombinant His- or GST-VCP protein was incubated with MBP-mock, MBP-Dorfin^{full}, MBP-Dorfin^{N}, MBP-Dorfin^{C}, and MBP-Parkin proteins *in vitro*. Two μg of His- or GST-VCP proteins and MBP fusion proteins at similar molar concentrations to VCP proteins were used for the assays. The amounts of MBP fusion and GST fusion Dorfin derivatives and His-VCP in 10% of the samples used are shown (*10% input*). *NTA*, nitrilotriacetic acid. *IB*, immunoblot. *B*, 2 μg of His-VCP was incubated with MBP-mock,

binding between Dorfin and VCP and to determine the exact portion of Dorfin that interacts with VCP *in vitro*, we performed pull-down assays using recombinant proteins. Recombinant MBP-Dorfin or its deletion mutants (*i.e.* MBP-Dorfin^{N} and MBP-Dorfin^{C}) and the same molar of recombinant His-VCP or GST-VCP were mixed and incubated for 1 h at 4 °C. MBP-mock protein was used as a negative control in these experiments. A small portion of MBP-Dorfin^{full} or Dorfin^{C} (C-terminal substrate-recognizing domain) bound to both His-VCP and GST-VCP, whereas MBP-mock, MBP-Dorfin^{N} (N-terminal RING-IBR domain), and MBP-Parkin did not bind to His-VCP or GST-VCP (Fig. 3*A*). We next determined the number of Dorfins that bind one hexamer of VCP. To investigate this issue, we incubated His-VCP with increasing amounts of MBP-Dorfin^{full}, MBP-Dorfin^{N}, MBP-Dorfin^{C}, MBP-mock, or MBP-Parkin. As shown in Fig. 3*B*, the amount of binding portion of MBP-Dorfin^{full} and -Dorfin^{C} pulled down with His-VCP was not saturated below the even molar ratio. The pull-down experiments using excess amounts of MBP-Dorfin^{full} revealed that MBP-Dorfin^{full} was saturated at the even molar ratio (Fig. 3*C*). As reported previously (15), recombinant His-VCP sedimented in high molecular weight fractions, indicating that it formed a hexamer *in vitro* (Fig. 3*D*). These findings indicated that six Dorfin molecules were likely bind to a VCP complex *in vitro*.

Subcellular Localization of Dorfin and VCP in HEK293 Cells—In previous studies, we showed that exogenous and endogenous Dorfin resided perinuclearly and was colocalized with Vimentin in cultured cells treated with a proteasome inhibitor (4). The staining patterns of Dorfin were indistinguishable from those of the aggresome, namely a pericentriolar, membrane-free, cytoplasmic inclusion containing misfolded ubiquitylated proteins packed in a cage of intermediate filaments (4). VCP immunostaining was also observed throughout aggresomes in cultured neuronal cells when induced by treatment with a proteasome inhibitor (15). In order to examine the subcellular localization of Dorfin and VCP, GFP-Dorfin and HA-VCP were co-expressed in HEK293 cells. Without proteasome treatment, GFP-Dorfin-expressing cells showed granular fluorescence in the cytosol, and the HA-VCP-expressing cells showed diffuse and uniform cytoplasmic staining (Fig. 4*A*). Treatment with MG132 (1 μM, 16 h) resulted in accumulation of both GFP-Dorfin and HA-VCP and perinuclear colocalization as a clear large protein aggregate that mimics aggresomes (Fig. 4*B*).

Colocalization of Dorfin and VCP in the Affected Neurons of ALS and PD—In previous studies, immunostaining of Dorfin and VCP was independently noted in LBs of PD, and the peripheral staining pattern of both proteins in LBs was similar (7, 23). To confirm the immunoreactivities of Dorfin and VCP in the affected neurons in ALS and PD, we performed a double-labeling immunofluorescence study using a rabbit polyclonal anti-Dorfin antibody (Dorfin-41) and a mouse monoclonal VCP antibody on the postmortem samples of ALS and PD. In the ALS spinal cords, both proteins were colocalized in the LB-like inclusions (Fig. 5, *A–F*). The margin of LBs in PD was intensely immunostained for Dorfin and VCP, and merged images confirmed their strong colocalization (Fig. 5, *G–L*). Dorfin and VCP were also positive in Lewy neurites in the affected neurons of PD (Fig. 5, *M–O*).

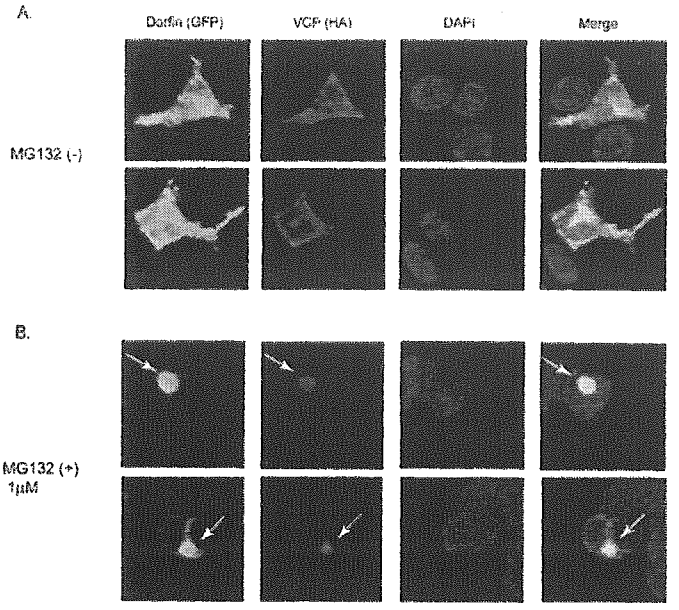

FIG. 4. **Subcellular localization of GFP-Dorfin and HA-VCP in HEK293 cells treated or untreated with a proteasome inhibitor.** GFP-Dorfin and HA-VCP were co-expressed transiently in HEK 293 cells. Cells were treated with (*B*) or without (*A*) 1 μM MG132 for 16 h. HA-VCP was stained with anti-monoclonal HA antibody (12CA5). Nuclei were stained with 4′,6-diamidino-2-phenylindole (*DAPI*). Without the treatment of MG132, GFP-Dorfin was spread through the cytosol, and it appeared like small aggregations. HA-VCP was also seen mainly in the cytosol and partly colocalized with GFP-Dorfin (*A*). After treatment with 1 μM MG132 for 16 h, both GFP-Dorfin and HA-VCP showed perinuclear accumulation and colocalization and appeared as clear large protein aggregates (*B*; *arrows*).

Dorfin Ubiquitylates Mutant SOD1 in Vivo—Unlike the wild-type form, mutant SOD1 proteins are rapidly degraded by the ubiquitin-proteasome system. Consistent with our previous results (5), SOD1^{G93A} and SOD1^{G85R} were polyubiquitylated, and co-expression with FLAG-Dorfin^{WT} enhanced polyubiquitylation of these mutant SOD1s compared with co-expression with FLAG-BAP, a negative control construct (Fig. 6*A*). Boiling with 1% SDS-containing buffer did not change the level of ubiquitylated mutant SOD1, indicating that mutant SOD1 itself was ubiquitylated by Dorfin (Fig. 6*B*). We also performed the same *in vivo* ubiquitylation assay using Neuro2a cells to examine for E3 activity of Dorfin in neuronal cells. The enhanced polyubiquitylation of these mutant SOD1s by Dorfin was observed in Neuro2a cells as well as in HEK293 cells (Fig. 6*C*). FLAG-Dorfin$^{C132S/C135S}$ did not enhance polyubiquitylation of mutant SOD1s, indicating that this RING finger mutant form was functionally inactive (Fig. 6*D*).

VCP^{K524A} Suppresses the E3 Activity of Dorfin—VCP has two ATPase binding domains (D1 and D2). A D2 domain mutant, VCP^{K524A}, induces cytoplasmic vacuoles, which mimics vacuole formation seen in the affected neurons in various neurodegenerative diseases (11, 15). The D2 domain represents the major ATPase activity and is essential for VCP function (11). The ATPase activity of VCP^{K524A} is much lower than that of VCP^{WT}, and VCP^{K524A} caused accumulation of polyubiquitylated proteins in the nuclear and membrane fractions together with elevation of ER stress marker proteins due to ERAD

MBP-Dorfin^{full}, MBP-Dorfin^{N}, MBP-Dorfin^{C}, and MBP-Parkin with increasing amounts (molar ratio to VCP: 0.25, 0.5, and 1.0). The amounts of MBP fusion Dorfin derivatives and His-VCP in 10% of the samples used are shown (10% input). *C*, 2 μg of His-VCP was incubated with MBP-Dorfin^{full} with increasing amounts (molar ratio to VCP: 0.25, 0.5, 1, 2, and 4). The amounts of MBP-Dorfin^{full} and His-VCP in 10% of the samples used are shown (*10% input*). *D*, His-VCP protein (0.5 μg) was fractionated by 10–40% glycerol gradient centrifugation followed by separation into 30 fractions using a fraction collector. Immunoblotting using anti-VCP antibody was performed on the selected fractions (fractions 2–17). *, The molar ratio was calculated by the amount of VCP monomers, not VCP complexes.

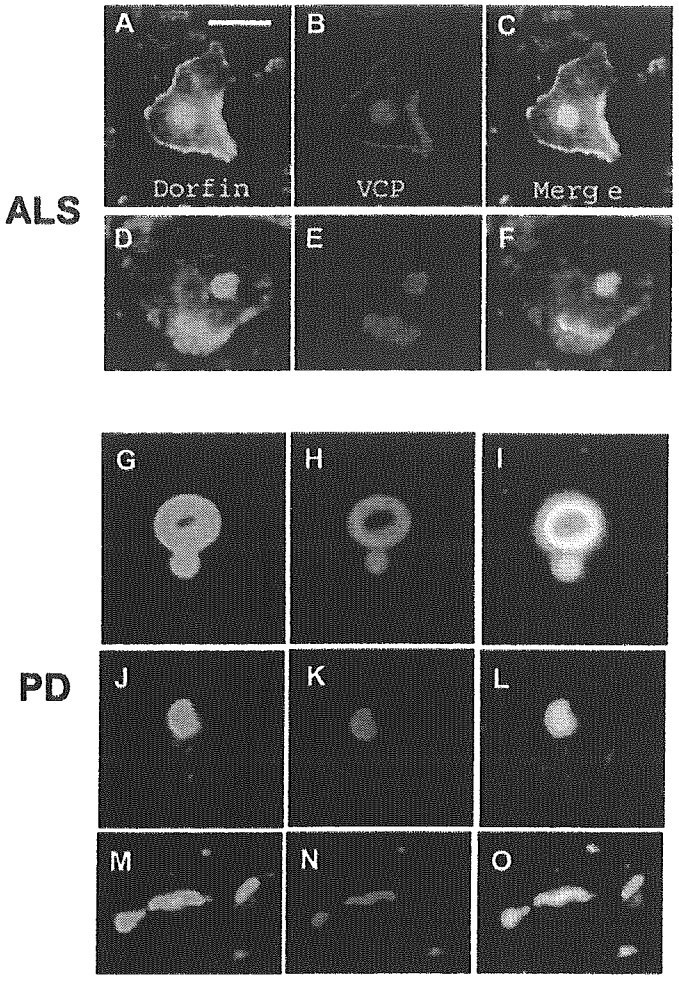

FIG. 5. **Colocalization of Dorfin-41 immunoreactivity with VCP in neuronal inclusions in ALS and PD.** Sections were doubly labeled with anti-Dorfin-41 antiserum and monoclonal VCP antibody and analyzed with a laser-scanning confocal microscope. The *left panels* (*green*) correspond to Dorfin, *middle panels* (*red*) correspond to VCP, and *right panels* correspond to merged images; structures in *yellow* indicate colocalization. Colocalization of Dorfin and VCP is seen in LB-like inclusions in motor neurons of the spinal cord of ALS (*A–F*). Dorfin is also colocalized with VCP in the margin of LBs (*G–I*), premature LBs (*J–L*), and Lewy neurites (*M–O*) in the nigral neurons of PD. *Scale bars*, 20 μm (*A–L*) and 10 μm (*M–O*).

inhibition, whereas its expression level, localization, and complex formation were indistinguishable from those of VCP^{WT} (11). In order to examine the functional effect of VCP on Dorfin, VCP^{WT}, VCP^{K524A}, or LacZ was co-expressed with $SOD1^{G85R}$, FLAG-Dorfin, and HA-Ub in HEK293 cells. Co-expression with VCP^{K524A} showed a marked decline of polyubiquitylation of $SOD1^{G85R}$ compared with co-expression with VCP^{WT} or LacZ (Fig. 7*A*, *top* and *middle*). Since Dorfin physically interacts with mutant SOD1s (5), we next investigated whether this decline of polyubiquitylation of $SOD1^{G85R}$ was mediated by reduced affinity between $SOD1^{G85R}$ and Dorfin. Immunoprecipitation by anti-FLAG antibody showed that VCP^{K524A} did not change affinity between $SOD1^{G85R}$ and Dorfin (Fig. 7*A*, *bottom*). Neither VCP^{WT} nor VCP^{K524A} changed the level of polyubiquitylation protein in the total lysate (Fig. 7*B*). To clarify whether this negative effect of VCP^{K524A} is specific for Dorfin, we assessed the autoubiquitylation of FLAG-Parkin in the presence of VCP^{WT}, VCP^{K524A}, or LacZ. Co-expression of VCP^{K524A} did not decrease autoubiquitylation of FLAG-Parkin compared with co-expression of LacZ or VCP^{WT} (Fig. 7*C*). We performed the same experiments using Neuro2a cells to see whether VCP^{K524A} suppress the E3 activity of Dorfin in neuronal cells. The marked decline of polyubiquitylation of $SOD1^{G85R}$ by VCP^{K524A} expression was also seen in Neuro2a cells (Fig. 7*D*).

DISCUSSION

UBIs in the affected neurons are histopathological hallmarks in various neurodegenerative disorders (8). Dorfin is an E3 ligase, which can ubiquitylate mutant SOD1s and synphilin-1 (5, 24). These substrates and Dorfin were identified in UBIs in various neurodegenerative diseases, such as LB-like inclusions in ALS and LBs in PD and dementia with Lewy bodies (7). This finding suggests that Dorfin may play a crucial role in the process of generating inclusions in the affected neurons. In the present study, we identified VCP as one of the Dorfin-associated proteins using mass spectrometry, and VCP-Dorfin physical interaction was confirmed by an immunoprecipitation experiment using FLAG-Dorfin and HA-VCP overexpressed in HEK293 cells (Fig. 1*A*). VCP is an essential and highly conserved protein of the AAA-ATPase family, which is considered to have diverse cellular functions, such as membrane fusion (25–27), nuclear trafficking (28), cell proliferation (29, 30), and the ERAD pathway (18–22). Many reports have implied that VCP is involved in the pathogenesis of various neuromuscular diseases. VCP has been implicated as a factor that modifies the progress of polyglutamine-induced neuronal cell death (15). In addition, histopathological studies revealed positive staining for VCP in UBIs in PD and ALS with dementia (23). VCP is also associated with MJD protein/atxin-3, in which abnormal expansion of polyglutamine tracts causes Machado-Joseph disease/spinocerebellar ataxia type 3 (31). VCP is also required for the degradation of ataxin-3 in collaboration with E4B/Ufd2a, a ubiquitin chain assembly factor (E4) (32). Recent studies have indicated that missense mutations in the VCP gene cause inclusion body myopathy associated with Paget's disease of bone and frontotemporal dementia, which is characterized by the presence of vacuoles in the cytoplasm in muscle fibers (33).

Our results showed that endogenous Dorfin formed a 400–600-kDa complex in various tissues and various cultured cells (Fig. 1*B*). Dorfin is a ~91-kDa protein; therefore, this high M_r complex should include Dorfin-associated proteins, although the possibility that Dorfin itself oligomerizes in the cell cannot be excluded. Glycerol gradient centrifugation analysis and immunoprecipitation experiments in the present study showed that endogenous Dorfin interacted with endogenous VCP in a complex of approximately 600 kDa, possibly including a Dorfin molecule and a hexametric form of VCP (Fig. 1*C*).

The first RING mutant of Dorfin, in which Cys at positions 132 and 135 changed to Ser, was prepared. This mutant Dorfin, $Dorfin^{C132S/C135S}$, could not ubiquitylate mutant SOD1s (Fig. 6*D*). Glycerol gradient centrifugation analysis revealed that $Dorfin^{C132S/C135S}$ did not form a high M_r complex, whereas exogenous wild type Dorfin ($Dorfin^{WT}$) formed a high M_r complex similar to endogenous Dorfin (Fig. 2*A*). Furthermore, an immunoprecipitation experiment using $Dorfin^{WT}$ and $Dorfin^{C132S/C135S}$ revealed that $Dorfin^{WT}$ could interact with VCP, whereas $Dorfin^{C132S/C135S}$ could not (Fig. 2*B*).

Our *in vitro* study using recombinant proteins showed that full-length ($MBP\text{-}Dorfin^{full}$) and the C terminus of Dorfin ($MBP\text{-}Dorfin^{C}$) directly interacted with VCP, whereas the $MBP\text{-}Dorfin^{N}$ mutant, containing the entire RING finger domain (amino acid residues 1–367), did not bind to VCP (Fig. 3*A*). This finding was unexpected, since *in vivo* binding analysis suggested that Dorfin could interact with VCP at the RING finger domain. It is plausible that certain structural changes in $Dorfin^{C132S/C135S}$ might render the C-terminal VCP-binding portion incapable of accessing VCP molecules. This may explain the result that $Dorfin^{C132S/C135S}$ did not form a high M_r complex.

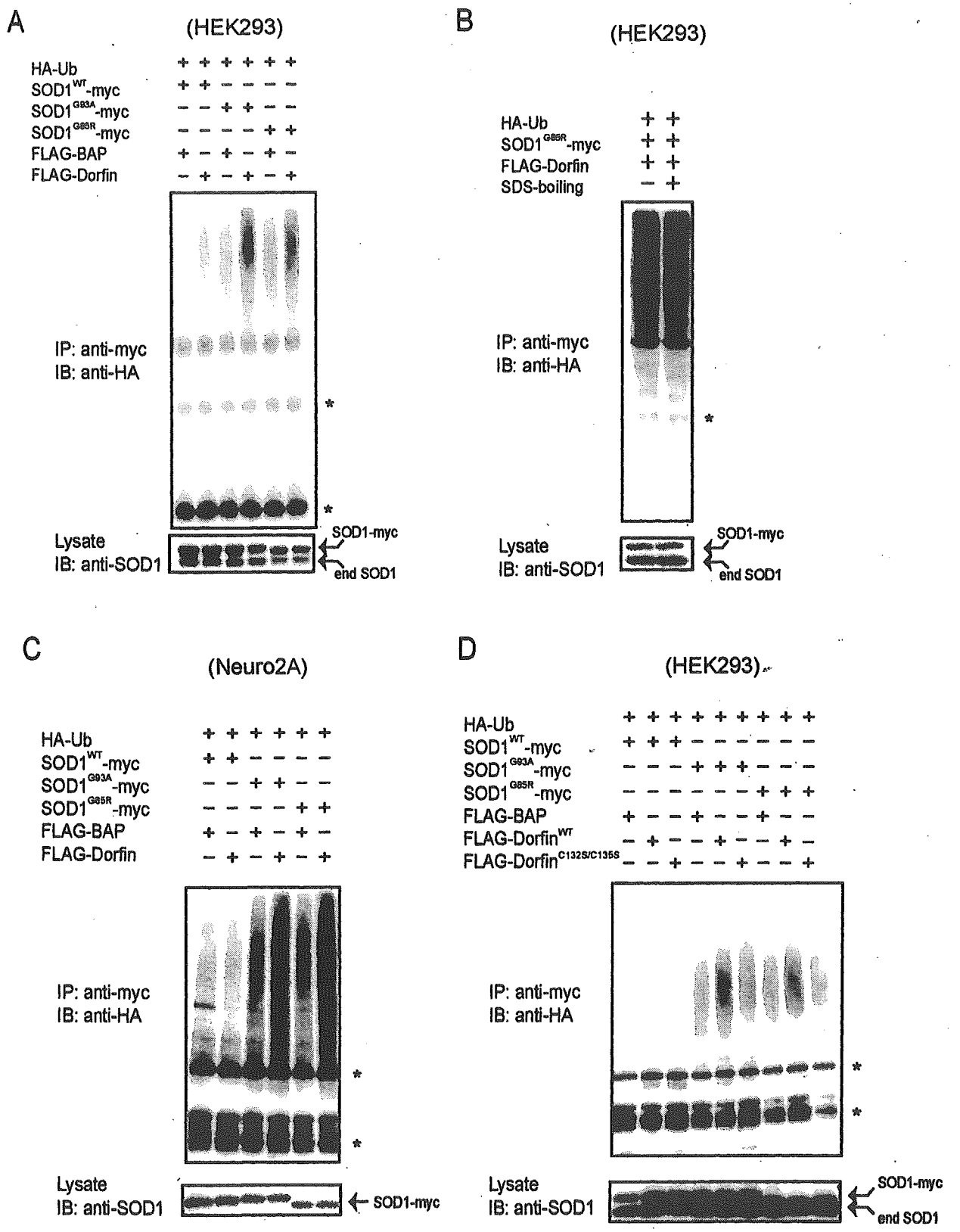

FIG. 6. **Dorfin ubiquitylates mutant SOD1s *in vivo*.** *A*, increased ubiquitylation of mutant SOD1 proteins by overexpression of Dorfin. HEK293 cells were co-transfected with $SOD1^{WT}$-Myc, $SOD1^{G93A}$-Myc, or $SOD1^{G85R}$-Myc and HA-Ub with or without FLAG-Dorfin. FLAG-bovine alkaline phosphatase (*BAP*) was used as a negative control. Immunoprecipitation (*IP*) was performed with Myc antibody (9E10). *IB*, immunoblotting. *B*, SDS boiling was performed prior to immunoprecipitation. To examine covalently ubiquitylated molecules, the cell lysate was boiled with the buffer containing 1% SDS for 5 min. Immunoprecipitation with Myc antibody (9E10) showed that the SDS-boiling procedure did not change polyubiquitylation level of $SOD1^{G85R}$-Myc by Dorfin. *C*, increased ubiquitylation of mutant SOD1 proteins by overexpression of Dorfin in Neuro2a cells. The same *in vivo* ubiquitylation assay as in *A* was performed using Neuro2a cells. *D*, $Dorfin^{C132S/C135S}$ ($Dorfin^{C132S/C135S}$) did not have E3 activity on mutant SOD1. HEK293 cells were co-transfected with $SOD1^{WT}$-Myc, $SOD1^{G93A}$-Myc, or $SOD1^{G85R}$-Myc and HA-Ub with FLAG-$Dorfin^{WT}$ or FLAG-$Dorfin^{C132S/C135S}$. The *asterisks* indicate IgG light and heavy chains.

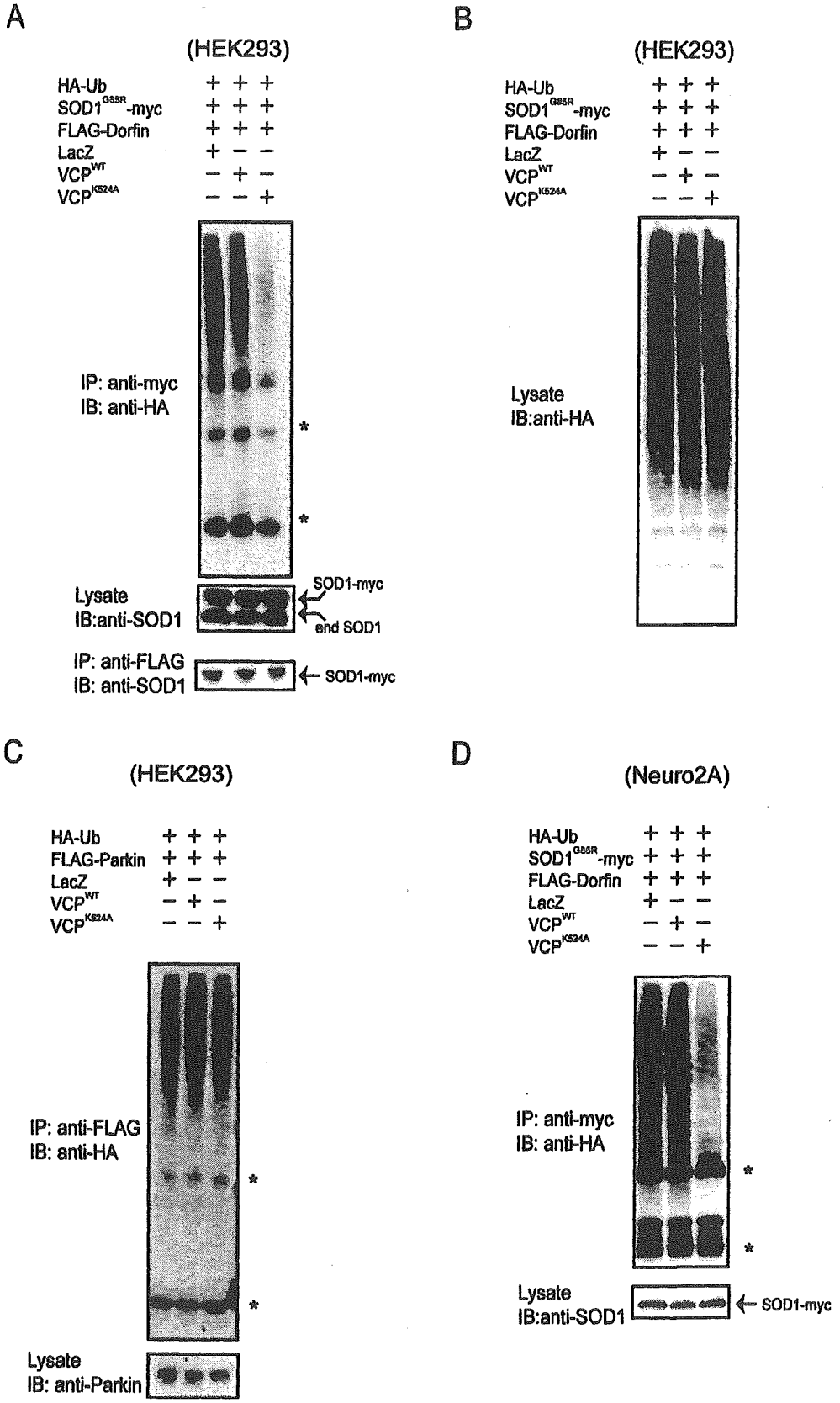

FIG. 7. **A dominant negative mutant of VCP, VCP^{K524A} inhibits the E3 ubiquitin ligase activity of Dorfin.** *A*, inhibition of dominant negative form mutant VCP^{K524A} on the E3 ubiquitin ligase activity of Dorfin. HEK293 cells were co-transfected with $SOD1^{G85R}$-Myc, HA-Ub, FLAG-Dorfin, and VCP^{WT}, VCP^{K524A}, or LacZ. Immunoprecipitation (*IP*) was performed with Myc antibody (9E10) and FLAG antibody (M2). *IB*, immunoblotting. *B*, neither VCP^{WT} nor VCP^{K524A} changed the level of total polyubiquitylated protein in the cell lysate. Ten percent of the volume of HEK293 cells used in *A* was subjected to immunoblotting using anti-HA (12CA5) antibody. *C*, autoubiquitylation of FLAG-Parkin was not influenced by the dominant negative form VCP^{K524A}. HEK293 cells were co-transfected with FLAG-Parkin, HA-Ub, and VCP^{WT}, VCP^{K524A}, or LacZ. Immunoprecipitation with FLAG antibody (M2) was performed. *D*, inhibition of VCP^{K524A} on E3 ubiquitin ligase activity of Dorfin in Neuro2a cells. Neuro2a cells were co-transfected with $SOD1^{G85R}$-Myc, HA-Ub, FLAG-Dorfin, and VCP^{WT}, VCP^{K524A}, or LacZ. Immunoprecipitation was performed using Myc antibody (9E10) and FLAG antibody (M2). The *asterisks* indicate IgG light and heavy chains.

The amount of Dorfin bound with VCP was saturated at even molar ratio *in vitro* (Fig. 3, *B* and *C*). Since VCP exists as a homohexamer (Fig. 3*D*), the *in vivo* observed size of ~600 kDa appears to be too small for the Dorfin-VCP complex if one VCP molecule binds to more than one Dorfin as shown in *in vitro* experiments. However, it is noteworthy that the size of molecules estimated by glycerol density gradient centrifugation analysis used in this study is not accurate and sufficient to discuss the molecular interaction of Dorfin and VCP in the cells. To date, various adaptor proteins, with which VCP forms multiprotein complexes, have been identified, such as Npl4, Ufd1 (18, 20), Ufd2 (34), Ufd3 (35), p47 (36), or SVIP (37). Although our *in vitro* study showed direct physical interaction between Dorfin and VCP, the environment with those adaptor proteins might reflect *in vivo* conditions. This also may explain the apparent discrepancy of the Dorfin-VCP binding fashions between *in vivo* and *in vitro* analyses.

Treatment with a proteasomal inhibitor causes the translocation of endogenous VCP and Dorfin to the aggresome in cultured cells (4, 15). Our results showed that these two proteins indeed colocalized perinuclearly in the aggresome following treatment with a proteasomal inhibitor (Fig. 4). Furthermore, we were able to demonstrate both Dorfin and VCP immunoreactivities in LB-like inclusions in ALS and LBs in PD (Fig. 5). In the majority of LBs, indistinguishable peripheral staining patterns were observed with both anti-Dorfin and anti-VCP antibodies. These results confirmed that both Dorfin and VCP are associated with the formation processes of aggresomes and inclusion bodies through physical interaction.

We showed here that co-expression of VCP^{K524A} resulted in a marked decrease of ubiquitylation activity of Dorfin compared with co-expression of VCP^{WT} or control. On the other hand, VCP^{K524A} failed to decrease autoubiquitylation activity of Parkin. VCP^{K524A} did not change the level of polyubiquitylated protein accumulation in the cell lysate in this study (Fig. 7). Knockdown experiments using the RNA interference technique showed accumulation of polyubiquitylated proteins (38). Combined with the observation that inhibition of VCP did not decrease the general accumulation of polyubiquitylated proteins, our results indicated that the E3 regulation function of VCP may be specific to certain E3 ubiquitin ligases such as Dorfin. VCP is an abundant protein that accounts for more than 1% of protein in the cell cytosol and is known to have various chaperone-like activities (39); therefore, it may function as a scaffold protein on the E3 activity of Dorfin. The localization of Dorfin and VCP in UBIs in various neurodegenerative disorders indicates the involvement of these proteins in the quality control system for abnormal proteins accumulated in the affected neurons in neurodegenerative disorders.

Since the unfolded protein response and ERAD are dynamic responses required for the coordinated disposal of misfolded proteins (40), the ERAD pathway can be critical for the etiology of neuronal cell death caused by various unfolded proteins. VCP is required for multiple aspects of the ERAD system by recognition of polyubiquitylated proteins and translocations to the 26 S proteasome for processive degradation through the VCP-Npl4-Ufd1 complex (18, 41). Our results suggest the involvement of Dorfin in the ERAD system, which is related to the pathogenesis of neurodegenerative disorders, such as PD or Alzheimer's disease. Further study including Dorfin knockout and/or knockdown models should examine the pathophysiology of Dorfin in association with the ERAD pathway or other cellular functions. Such studies should enhance our understanding of the pathogenetic role of Dorfin in neurodegenerative disorders.

REFERENCES

1. Julien, J. P. (2001) *Cell* **104**, 581–591
2. Rowland, L. P., and Shneider, N. A. (2001) *N. Engl. J. Med.* **344**, 1688–1700
3. Ishigaki, S., Niwa, J., Ando, Y., Yoshihara, T., Sawada, K., Doyu, M., Yamamoto, M., Kato, K., Yotsumoto, Y., and Sobue, G. (2002) *FEBS Lett.* **531**, 354–358
4. Niwa, J., Ishigaki, S., Doyu, M., Suzuki, T., Tanaka, K., and Sobue, G. (2001) *Biochem. Biophys. Res. Commun.* **281**, 706–713
5. Niwa, J., Ishigaki, S., Hishikawa, N., Yamamoto, M., Doyu, M., Murata, S., Tanaka, K., Taniguchi, N., and Sobue, G. (2002) *J. Biol. Chem.* **277**, 36793–36798
6. Ciechanover, A., and Brundin, P. (2003) *Neuron* **40**, 427–446
7. Hishikawa, N., Niwa, J., Doyu, M., Ito, T., Ishigaki, S., Hashizume, Y., and Sobue, G. (2003) *Am. J. Pathol.* **163**, 609–619
8. Mayer, R. J., Lowe, J., Lennox, G., Doherty, F., and Landon, M. (1989) *Prog. Clin. Biol. Res.* **317**, 809–818
9. Johnston, J. A., Ward, C. L., and Kopito, R. R. (1998) *J. Cell Biol.* **143**, 1883–1898
10. Kopito, R. R. (2000) *Trends Cell Biol.* **10**, 524–530
11. Kobayashi, T., Tanaka, K., Inoue, K., and Kakizuka, A. (2002) *J. Biol. Chem.* **277**, 47358–47365
12. Shimura, H., Hattori, N., Kubo, S., Mizuno, Y., Asakawa, S., Minoshima, S., Shimizu, N., Iwai, K., Chiba, T., Tanaka, K., and Suzuki, T. (2000) *Nat. Genet.* **25**, 302–305
13. Fukuchi, M., Imamura, T., Chiba, T., Ebisawa, T., Kawabata, M., Tanaka, K., and Miyazono, K. (2001) *Mol. Biol. Cell* **12**, 1431–1443
14. Ishigaki, S., Liang, Y., Yamamoto, M., Niwa, J., Ando, Y., Yoshihara, T., Takeuchi, H., Doyu, M., and Sobue, G. (2002) *J. Neurochem.* **82**, 576–584
15. Hirabayashi, M., Inoue, K., Tanaka, K., Nakadate, K., Ohsawa, Y., Kamei, Y., Popiel, A. H., Sinohara, A., Iwamatsu, A., Kimura, Y., Uchiyama, Y., Hori, S., and Kakizuka, A. (2001) *Cell Death Differ.* **8**, 977–984
16. Natsume, T., Yamauchi, Y., Nakayama, H., Shinkawa, T., Yanagida, M., Takahashi, N., and Isobe, T. (2002) *Anal. Chem.* **74**, 4725–4733
17. Matsuda, N., Suzuki, T., Tanaka, K., and Nakano, A. (2001) *J. Cell Sci.* **114**, 1949–1957
18. Bays, N. W., and Hampton, R. Y. (2002) *Curr. Biol.* **12**, R366–R371
19. Ye, Y., Meyer, H. H., and Rapoport, T. A. (2001) *Nature* **414**, 652–656
20. Braun, S., Matuschewski, K., Rape, M., Thoms, S., and Jentsch, S. (2002) *EMBO J.* **21**, 615–621
21. Jarosch, E., Taxis, C., Volkwein, C., Bordallo, J., Finley, D., Wolf, D. H., and Sommer, T. (2002) *Nat. Cell Biol.* **4**, 134–139
22. Rabinovich, E., Kerem, A., Frohlich, K. U., Diamant, N., and Bar-Nun, S. (2002) *Mol. Cell. Biol.* **22**, 626–634
23. Mizuno, Y., Hori, S., Kakizuka, A., and Okamoto, K. (2003) *Neurosci. Lett.* **343**, 77–80
24. Ito, T., Niwa, J., Hishikawa, N., Ishigaki, S., Doyu, M., and Sobue, G. (2003) *J. Biol. Chem.* **278**, 29106–29114
25. Meyer, H. H., Kondo, H., and Warren, G. (1998) *FEBS Lett.* **437**, 255–257
26. Kondo, H., Rabouille, C., Newman, R., Levine, T. P., Pappin, D., Freemont, P., and Warren, G. (1997) *Nature* **388**, 75–78
27. Rabouille, C., Kondo, H., Newman, R., Hui, N., Freemont, P., and Warren, G. (1998) *Cell* **92**, 603–610
28. Hetzer, M., Meyer, H. H., Walther, T. C., Bilbao-Cortes, D., Warren, G., and Mattaj, I. W. (2001) *Nat. Cell Biol.* **3**, 1086–1091
29. Frohlich, K. U., Fries, H. W., Rudiger, M., Erdmann, R., Botstein, D., and Mecke, D. (1991) *J. Cell Biol.* **114**, 443–453
30. Asai, T., Tomita, Y., Nakatsuka, S., Hoshida, Y., Myoui, A., Yoshikawa, H., and Aozasa, K. (2002) *Jpn. J. Cancer Res.* **93**, 296–304
31. Kawaguchi, Y., Okamoto, T., Taniwaki, M., Aizawa, M., Inoue, M., Katayama, S., Kawakami, H., Nakamura, S., Nishimura, M., Akiguchi, I., Kimura, J., Narumiya, S., and Kakizuka, A. (1994) *Nat. Genet.* **8**, 221–228
32. Matsumoto, M., Yada, M., Hatakeyama, S., Ishimoto, H., Tanimura, T., Tsuji, S., Kakizuka, A., Kitagawa, M., and Nakayama, K. I. (2004) *EMBO J.* **23**, 659–669
33. Watts, G. D., Wymer, J., Kovach, M. J., Mehta, S. G., Mumm, S., Darvish, D., Pestronk, A., Whyte, M. P., and Kimonis, V. E. (2004) *Nat. Genet.* **36**, 377–381
34. Koegl, M., Hoppe, T., Schlenker, S., Ulrich, H. D., Mayer, T. U., and Jentsch, S. (1999) *Cell* **96**, 635–644
35. Ghislain, M., Dohmen, R. J., Levy, F., and Varshavsky, A. (1996) *EMBO J.* **15**, 4884–4899
36. Meyer, H. H., Wang, Y., and Warren, G. (2002) *EMBO J.* **21**, 5645–5652
37. Nagahama, M., Suzuki, M., Hamada, Y., Hatsuzawa, K., Tani, K., Yamamoto, A., and Tagaya, M. (2003) *Mol. Biol. Cell* **14**, 262–273
38. Wojcik, C., Yano, M., and DeMartino, G. N. (2004) *J. Cell Sci.* **117**, 281–292
39. Dalal, S., and Hanson, P. I. (2001) *Cell* **104**, 5–8
40. Travers, K. J., Patil, C. K., Wodicka, L., Lockhart, D. J., Weissman, J. S., and Walter, P. (2000) *Cell* **101**, 249–258
41. Dai, R. M., and Li, C. C. (2001) *Nat. Cell Biol.* **3**, 740–744

Neuroscience 129 (2004) 109–117

WIDE RANGE OF LINEAGES OF CELLS EXPRESSING NERVE GROWTH FACTOR mRNA IN THE NERVE LESIONS OF PATIENTS WITH VASCULITIC NEUROPATHY: AN IMPLICATION OF ENDONEURIAL MACROPHAGE FOR NERVE REGENERATION

N. MITSUMA, M. YAMAMOTO, M. IIJIMA, N. HATTORI, Y. ITO, F. TANAKA AND G. SOBUE*

Department of Neurology, Nagoya University Graduate School of Medicine, 65 Tsurumai, Showa-ku, Nagoya 466-8550, Japan

Abstract—*In situ* localization of nerve growth factor (NGF) mRNA was examined in the nerve lesions of patients with vasculitic neuropathy. Double labeling of *in situ* hybridization for NGF mRNA and immunohistochemistry for cell markers showed that NGF mRNA was expressed in a wide range of lineages of cells: Schwann cells, infiltrating macrophages, T cells and perivascular cells. Round-shaped macrophages with early-phase features expressed high levels of NGF mRNA, in contrast to late-phase polymorphic macrophages, which expressed low levels of NGF mRNA. NGF mRNA was also expressed universally in T cells with various cell surface markers. Epineurial macrophages surrounding vasculitic lesions and endoneurial T cells expressed high levels of NGF mRNA in the damaged nerves. Moreover, the extent of endoneurial NGF expression level in macrophages was closely related to the degree of axonal regeneration. These results suggest that NGF is expressed in a wide range of lineages of cells but is differentially expressed spatially in vasculitic nerve lesions, and that the expressed NGF, particularly in macrophages, may play an important role in the nerve regeneration process.

Key words: nerve growth factor, macrophages, T cells, Schwann cells, vasculitic neuropathy.

Numerous neurotrophic factors and cytokines are produced in nerve lesions of various neuropathies. They form a multi-factorial regulation network in lesions in the acute and chronic phase and function in nerve regeneration. Cell-type-specific trophic activity and production of neurotrophic factors have been reported (Snider and Wright, 1996; Molliver et al., 1997). We have previously demonstrated that the neurotrophic factors and cytokines are up- or down-regulated temporally in the nerve lesions in human neuropathies as well as in rodent neuropathic models (Sobue et al., 1988, 1998; Ito et al., 1998).

Among these factors, nerve growth factor (NGF) is considered to play an important role in recovery of neuropathy. NGF was found as a protein influencing nerve growth in the 1950s, and is known to affect sensory neurons of dorsal root ganglia (DRG), autonomic sympathetic neurons, and basal forebrain cholinergic neurons (Levi-Montalcini et al., 1996). NGF and other related neurotrophic factors structurally similar to NGF form a family of neurotrophins that bind to their cognate specific high-affinity receptors, which contain a tyrosine kinase domain, and also bind to low-affinity receptor p75 (Hantzopoulous et al., 1994). NGF binds to its high-affinity receptor TrkA, which interacts with p75 as a positive modulator for myelination, in order to promote neurotrophic effects by activating signaling pathways initiated by tyrosine kinase activity (Chao and Hempstead, 1995; Cosgaya et al., 2002).

NGF has a neurotrophic effect on neuropathies in animal and explant models caused by physical and chemical damage (Miyata et al., 1986; Hayakawa et al., 1998; Fischer et al., 2001). When NGF is administered prior to experimental neuropathy caused by axotomy, NGF promotes survival and regeneration of neurons (Rich et al., 1987; Apfel et al., 1992). NGF expression in the lesions of experimental neuropathy shows a two-peaked up-regulation pattern in the cut-crush mouse model (Heumann et al., 1987; Ito et al., 1998). This expression pattern is caused by infiltrating cells at the first peak, and then by lesioned Schwann cells at the second peak. TrkA and p75 are also up-regulated and maintained after nerve crush injury (Greeson et al., 1992; Yamamoto et al., 1998a).

The histopathological expression profile of NGF in the lesions of human neuropathies is not yet fully understood. In nerve lesions of human neuropathies, various types of pathology including inflammatory, ischemic, and metabolic changes, are present in different phases. In necrotizing vasculitic neuropathies, nerve pathology consists almost exclusively of axonal degeneration with Wallerian degeneration due to ischemic damages (Hawke et al., 1991; Hattori et al., 1999). We previously reported that NGF mRNA expression was increased in nerve lesions of vasculitic neuropathies, and that the increase was well correlated with the extent of invasion of macrophages and T cells (Yamamoto et al., 2001). Investigation of the histopathological distribution of NGF mRNA will help to advance our understanding of the mechanism of nerve regeneration by NGF, and be of importance from the point of view of clinical therapeutic implications. In this study we examined the histopathological localization of NGF mRNA in nerves of patients with vasculitic neuropathies using double staining consisting of *in situ* NGF hybridization and immunohistochemistry against various types of cell-specific markers, and here we report those re-

*Corresponding author. Tel: +81-52-744-2385; fax: +81-52-744-2384.
E-mail address: sobueg@med.nagoya-u.ac.jp (G. Sobue).
Abbreviations: CT, computed tomography; DRG, dorsal root ganglion; MRI, magnetic resonance imaging; NGF, nerve growth factor.

0306-4522/04$30.00+0.00
doi:10.1016/j.neuroscience.2004.06.083

Table 1. Clinical features of patients[a]

Diagnosis	No. of cases	Age (years)	Sex (M/F)	Duration prior to biopsy (days)
Microscopic polyangiitis	5	64.8±17.5 (44–84)	2/3	5.6 (2–8)
Non-systemic vasculitic neuropathy	3	67.5±3.5 (64–71)	2/1	7.3 (2–14)
Normal-appearing nerves	5	63.2±5.6 (56–76)	3/2	–

[a] Age is expressed as mean±S.D. (range). Duration prior to biopsy is expressed as mean (range). –, not applicable.

sults and discuss the role of NGF produced in different cell types.

EXPERIMENTAL PROCEDURES

Patients and sural nerve biopsies

Sural nerve specimens were obtained from diagnostic sural nerve biopsies from eight patients with vasculitic neuropathies (four women, four men; mean age, 66.6 years; age range, 44–84 years). The patients consisted of five patients with microscopic polyangiitis and three with non-systemic vasculitic neuropathy (Table 1). Patients underwent neurological assessment, cerebrospinal fluid analysis, cranial magnetic resonance imaging (MRI) computed tomography (CT), routine blood and urine studies, nerve conduction studies, sural nerve biopsies and therapeutic trials with corticosteroids. The diagnosis of the various categories of vasculitic neuropathy was based on the criteria adopted by the Chapel Hill Consensus Conference in 1994 (Jennette et al., 1994). Sural nerve biopsies were performed within 2 weeks (usually 1 week) after the onset of neuropathy prior to treatment (2–14 days, mean 6.5 days), and the samples were histologically examined as described previously (Hattori et al., 1999). Five sural nerve specimens with normal morphology were obtained from age-matched (56–76 years) individuals and served as controls. Informed consent was obtained from each patient. The study was approved by the ethics committee of Nagoya University Graduate School of Medicine.

Pathologic study

Other portions of the nerve segments were processed to prepare glutaraldehyde-fixed, epoxy-resin embedded semithin sections and formalin-fixed, paraffin-embedded sections to assess the morphology of the nerve fibers and any invading cells. Specimens were fixed in 2% glutaraldehyde in 0.025 M cacodylate buffer at pH 7.4, and processed for semithin, ultrathin, or teased-fiber studies. The density of myelinated fibers was assessed directly from the Toluidine Blue-stained semithin transverse sections of sural nerves using a computer-assisted image analyzer (Luzex FS; Nikon, Tokyo, Japan) as described previously (Sobue et al., 1988, 1998; Hattori et al., 1999). Teased fibers were isolated from one portion of glutaraldehyde-fixed specimens, and the pathological condition of each isolated fiber was evaluated (Sobue et al., 1988, 1998; Hattori et al., 1999). Axonal histopathologic features analyzed include axonal loss, and axonal degeneration in the teased-fiber preparations. In the transverse sections, clusters of two or three small myelinated fibers surrounded by basal lamina were designated as axonal regenerating sprouts, as described previously (Hattori et al., 1999; Koike et al., 2001). The population of fibers manifesting active axonal degeneration or a normal appearance per square millimeter was assessed by calculating the incidence of such fibers multiplied by the total population of myelinated fibers per square millimeter as described previously (Yamamoto et al., 1998b).

In situ hybridization, immunohistochemical study and quantitative analyses

One portion of the sural nerve specimens was immediately frozen in liquid nitrogen and stored at −80 °C until use. Ten-micrometer thick frozen sections of sural nerves were prepared for *in situ* hybridization and immunohistochemical staining. Frozen sections were treated with proteinase K, refixed in 4% paraformaldehyde, and processed for *in situ* hybridization and immunohistochemistry. For *in situ* hybridization, digoxigenin-labeled cRNA probes were generated from linearized plasmids for NGF using SP6 or T7 RNA polymerase (Roche Diagnostics, Basel, Switzerland). Sliced sural nerves were hybridized for 16 h at 40 °C with the probes in a solution (50% formamide, 10 mM Tris–HCl, pH 7.6, 1 mM EDTA, 0.6 M NaCl, 0.25% SDS, 0.1 mg/ml yeast tRNA, 10% dextran sulfate, and 1× Denhardt's solution), washed and detected immunologically with alkaline phosphatase- or FITC-conjugated anti-digoxigenin antibody. Immunohistochemistry was performed by the ABC method for rhodamine signals according to the manufacturer's protocol, using antibodies against the following cell-specific markers: S100 (Sigma) antibody for Schwann cells; CD68 (DAKO), MRP14 (Dianova) and MRP8 (Dianova) for macrophages; CD4 (DAKO), CD8 (DAKO), UCHL-I (DAKO) and CD3 (DAKO) for T-cells. The cell infiltrates immunoreactive for macrophage marker (CD68) and T cell marker (UCHL-1) were counted to assess the degree of inflammatory cell invasion in the epineurial and endoneurial areas of the nerve segments.

To assess the degree of NGF mRNA expression in the nerve segments, the signal intensity of NGF mRNA was quantified using a CCD image analyzer (Zeiss Axiovert S100TV) as previously described (Mitsuma et al., 1999; Yamamoto et al., 2001). Perivascular inflammatory lesions in the epineurium were identified as regions of infiltrating cells surrounding necrotizing vasculitic vessels, in most cases vessel walls (from intima to adventitia) of vasculitic vessels. Lesions in the endoneurium were also identified as regions of nerve fiber damage accompanied by infiltrating cells. Within these lesions, macrophages (CD68-positive cells), T cells (UCHL-1-positive cells), Schwann cells (S-100-positive cells), and antigen-specific cells with different profiles (MRP-14-, MRP-8-, CD3-, CD4-, and CD8-positive cells) were identified and assessed to determine the cellular profiles of active lesions in vasculitic neuropathy. The cells with cell-specific markers and NGF mRNA signals were assessed on the captured images of the desired magnification using a fluorescence microscope with a CCD image analyzer and image analyzing software (NIH image): approximately 300 MRP-14-positive cells, 200 MRP-8-positive cells, 100 CD3-positive positive cells, 100 CD4-positive positive cells, and 100 CD8-positive positive cells were observed per lesion of interest. The frequency of a specific lineage of cells (MRP14, MRP8, CD3, CD4, CD8 or S100) producing NGF mRNA was quantified as the percentage of cells with NGF mRNA signals among the total cells with the cell-specific marker. The signal intensity of cell-lineage-specific NGF mRNA was quantified by measuring cellular NGF mRNA signals with the cell-specific marker in the lesion of interest (100×100 μm), and expressed as NGF mRNA signals per square millimeter for each specific lineage of cells in the epineurium and endoneurium.

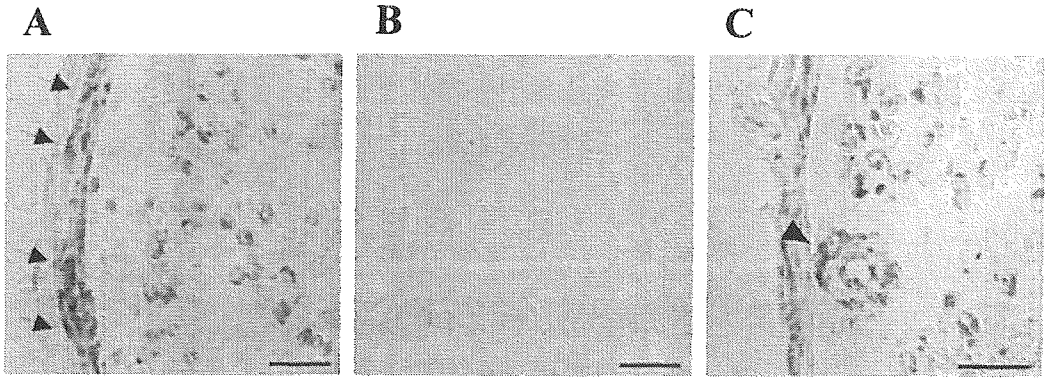

Fig. 1. *In situ* hybridization of NGF mRNA in vasculitic neuropathy. *In situ* hybridization with anti-sense (A and C) and sense probes (B) is shown. *In situ* hybridization of NGF mRNA indicated that NGF mRNA was expressed in the endoneurium and perineurium (arrows). Arrowhead indicates that perivascular cells expressed NGF mRNA. Scale bars=50 μm (A and B); 30 μm (C).

Statistical analysis

For statistical analysis, the Mann-Whitney *U* test was used for comparison of *in situ* mRNA levels between pairs of individual groups. A simple correlation test was performed for correlation analysis.

RESULTS

NGF mRNA expression in a wide range of lineages of cells in nerve lesions

In vasculitic neuropathies, NGF mRNA signals were observed in the endoneurium and epineurium, where vessel wall cells were also positive for NGF mRNA (Fig. 1), whereas in control nerves only the endoneurial cells were slightly positive for NGF mRNA. NGF mRNA was also detected in the perineurial cells in vasculitic neuropathies (Fig. 1). Fluorescent double staining of NGF mRNA and cell-specific antigens revealed that NGF mRNA was highly expressed in macrophages, T cells and Schwann cells.

Macrophage marker staining showed that the expression level of NGF mRNA in round or oval shaped macrophages was higher than that in polymorphic macrophages (Fig. 2A–F). NGF mRNA levels in MRP14+ macrophages (Fig. 2G–I) were higher than those in MRP8+ cells (Fig. 2J–L). NGF mRNA expression levels, which were expressed as signal intensities per square millimeter and percentages of cells with NGF signals, were higher in MRP14+ macrophages compared with MRP8+ macrophages in the endoneurial lesions accompanying active axonal degeneration (Figs. 3A and 4A). NGF mRNA expression in MRP8+ macrophages was significantly greater in the epineurial space than in the endoneurial space, but that in MRP14+ macrophages did not differ between the epineurial and endoneurial spaces (Figs. 3A and 4A). Furthermore, overall NGF mRNA signal intensity, expressed as signal intensity per square millimeter, did not differ significantly between MRP8− and MRP14+ macrophages in the epineurial lesions (Fig. 4A).

T cells with various cell surface markers expressed NGF mRNA (Fig. 2M–R). T cells expressed strong signals of NGF mRNA regardless of their surface markers, and almost all T cells produced NGF mRNA, especially in the endoneurial space (Fig. 3 B). The proportions of epineurial CD4, CD8, or CD3 immunoreactive cells expressing NGF mRNA were slightly lower as compared with those of the corresponding endoneurial T cells (Fig. 3B). Since the proportions of T cell subtypes were similar in the endoneurial and epineurial lesions, the overall levels of NGF mRNA signals of each T cell subtype did not significantly differ from each other (Fig. 4B).

S100-immunopositive Schwann cells expressed NGF mRNA in the diseased nerves, whereas in control nerves NGF mRNA was expressed at a low level in Schwann cells (Figs. 2S–U, 3C and 4C). Even in the nerve lesions, the NGF mRNA signals of Schwann cells themselves were lower than those of the infiltrating cells, but the overall signal count was high due to the relatively higher Schwann cell population in neuropathic lesions (Fig. 4C). Moreover, NGF mRNA was also present in vessel wall cells in both the epineurium and endoneurium.

NGF mRNA was expressed in macrophages and T cells in perivascular lesions of the epineurial space, while in the endoneurium, Schwann cells, in addition to invading cells, synthesized NGF mRNA. The overall intensity of NGF mRNA levels per area in the endoneurium was high in Schwann cells and MRP14+ macrophages compared with other cell types, including T cells (Fig. 4). On the other hand, MRP14+ and MRP8+ macrophages were major cell types expressing NGF mRNA in the epineurial lesions.

NGF mRNA expression and nerve regeneration

Pathological findings in the sural nerves of individual patients who had various vasculitic neuropathies and displayed the different NGF mRNA expression patterns are shown in Table 2. The pathological findings were highly variable among the patients, and independent of the underlying diseases causing vasculitic neuropathies. Axonal degeneration characteristic of vasculitic neuropathies was seen in all the patients, and axonal sprouts of regeneration were also associated with axonal pathology. The patients with more axonal sprouts demonstrated higher NGF mRNA levels not only in the endoneurium but also in the epineurium, as compared with those with fewer axonal sprouts (Fig. 5A and B). The endoneurial NGF mRNA

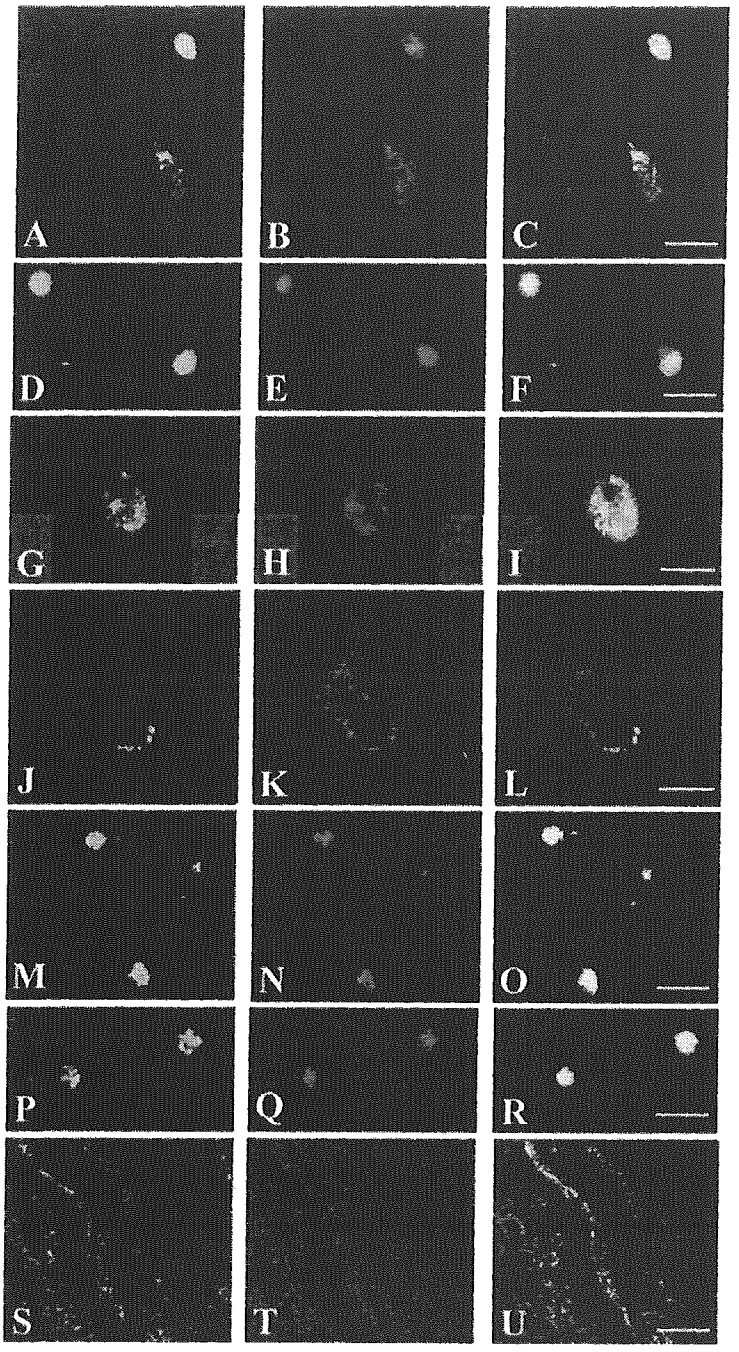

Fig. 2. Representative double staining of NGF mRNA in cells with various cell-specific markers. Double staining (merged yellow) of cells with various cell-specific markers (red) and NGF mRNA (green) is shown. NGF mRNA was strongly expressed in round and MRP14+ macrophages. T cells expressed strong signals of NGF mRNA. NGF mRNA signals in Schwann cells were weaker than those in the infiltrating cells. (A–C) Epineurial CD68+ cells; (D–F) endoneurial CD68+ cells; (G–I) endoneurial MRP14+ cell; (J–L) endoneurial MRP8+ cell; (M–O) epineurial UCHL-1+ cells; (P–R) endoneurial CD8+ cells; (S–U) S100+ cells. Scale bars=15 μm (A–F); 5 μm (G–L); 10 μm (M–R); 30 μm (S–U).

expression was more significantly correlated with axonal regenerating sprouts than epineurial one (r=0.84, P<0.01 vs. r=0.52, P=0.18). Furthermore, *in situ* Schwann cell NGF mRNA levels were correlated with the extent of axonal sprouts (r=0.75, P<0.05, Fig. 5C). The degree of NGF mRNA expression was well correlated with the extent of active axonal sprouting, but not with that of axonal degeneration, independent of the distribution of NGF mRNA expression.

DISCUSSION

NGF is known to support mainly small-diameter sensory neurons in DRG, and to express tropic activity for small

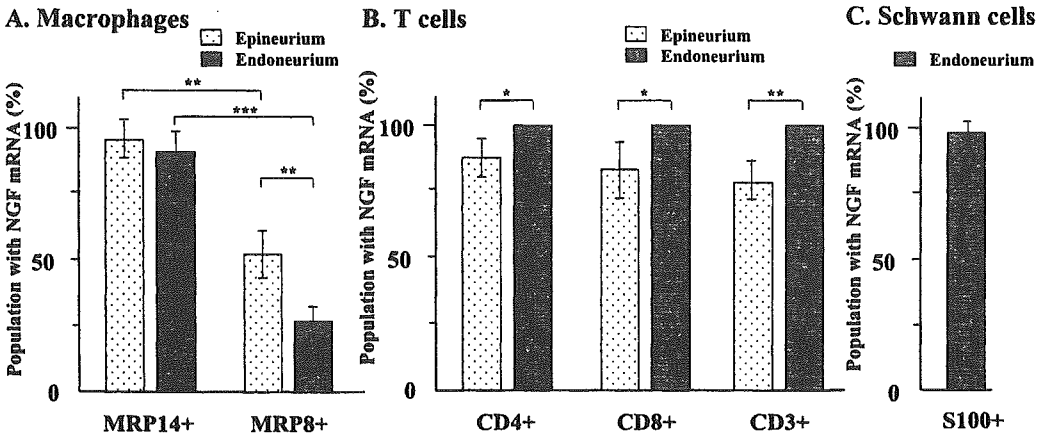

Fig. 3. Cell populations with NGF mRNA in the epineurial and endoneurial spaces. The cell populations with NGF mRNA signals and cell-specific markers were quantified as described in the text, and were expressed as percentages of cells with NGF mRNA signals in the epineurium and endoneurium in each patient. Mean±S.E. from the eight patients is indicated. * $P<0.05$, ** $P<0.01$, *** $P<0.001$.

myelinated and unmyelinated fibers of sensory nerves even in the adults (Rich et al., 1984; Unger et al., 1998). The high-affinity receptor TrkA for NGF is expressed in these neurons and their axons, but Schwann cells associated with small myelinated and unmyelinated fibers do not express TrkA. We demonstrated here for the first time the histological localization of NGF mRNA expression in the nerves of human neuropathy, using double staining with FITC and rhodamine to detect NGF mRNA and cell-specific antigens, respectively. NGF mRNA was expressed in the infiltrating macrophages and T cells, Schwann cells and perivascular cells in the nerve lesions. Expression of NGF mRNA in the infiltrating cells and other cells varied depending on the histological profiles and cell types. We have previously reported that in vasculitic neuropathies, the expression of NGF mRNA changed to a variable extent, and the mean levels of NGF mRNA were markedly increased compared with those of controls (Yamamoto et al., 2001). We also showed previously by a multiple regression analysis that NGF mRNA expression in the nerve lesions was closely related to the invasion of macrophages and T cells (Yamamoto et al., 2001). Our previous study using whole nerve homogenates, however, failed to determine which specific lineages of cells express NGF mRNA to what extent, and how cell-type-specific NGF expression is correlated with axonal pathology.

Macrophage recruitment is an important component of NGF synthesis and of sensory axon maintenance and re-growth (Brown et al., 1991; Luk et al., 2003). Endoneurial infiltration by macrophages is observed in Wallerian degeneration as well as in autoimmune polyneuropathies, which show phenotypic and functional heterogeneity of macrophages with respect to morphology, specific marker antigens and residency (Kiefer et al., 1998). The expression of NGF mRNA was higher in oval or round-shaped macrophages than in macrophages with an irregular or ramified appearance. Round-shaped macrophages are reported to be activated for secretion of humoral immune factors such as cytokines, whereas irregular-shaped mac-

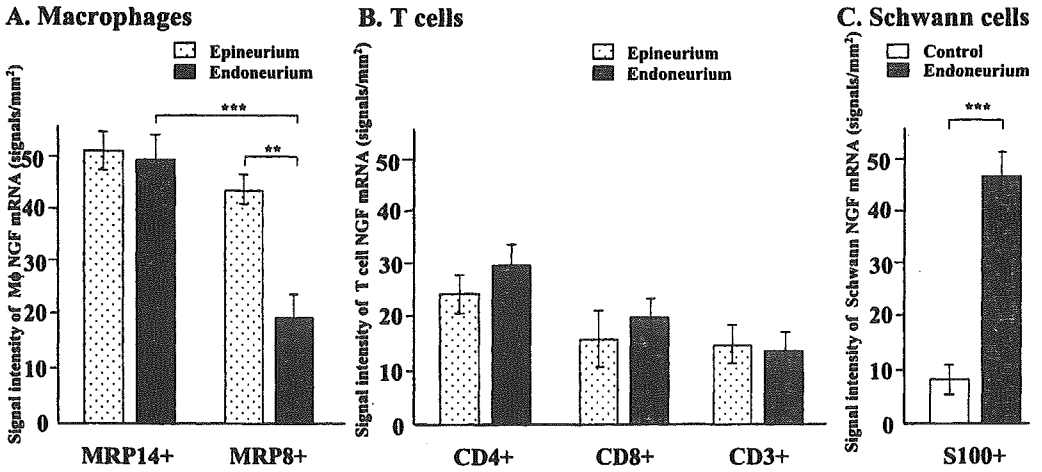

Fig. 4. Signal intensity of NGF mRNA in the epineurial and endoneurial macrophages, T cells and Schwann cells.The intensity of NGF mRNA signals with specific cell-specific markers was quantified as described in the text, and was expressed as signal intensity per square millimeter in the epineurium and endoneurium in each patient. Mean±S.E. from the eight patients and five controls is indicated. The white bar in C denotes Schwann cell expression of NGF mRNA in control nerves. * $P<0.05$, ** $P<0.01$, *** $P<0.001$.

Table 2. Pathological findings of sural nerve biopsies in the patients with vasculitic neuropathies[a]

Case	Age (years)/Sex	Diagnosis	MF density (No./mm^2)	Axonal degeneration (%)	Active axonal degeneration (No./mm^2)	Axonal regeneration: sprouts (No./mm^2)	Infiltrates in epineurium Mϕ/T cells (No./mm^2)	Infiltrates in endoneurium Mϕ/T cells (No./mm^2)
1	44/M	MP	2884	14	404	193	228/28	213/24
2	84/F	MP	909	95	864	59	352/19	323/38
3	66/F	MP	3081	9	277	262	449/38	407/25
4	51/F	MP	303	93	282	53	511/51	272/15
5	79/M	MP	1264	98	1239	93	288/20	148/8
6	71/M	Non-systemic	7467	4	299	15	215/12	181/9
7	74/F	Non-systemic	6557	33	2163	30	318/18	151/9
8	64/M	Non-systemic	3318	93	3086	10	189/15	88/11

[a] Active axonal degeneration, axonal degeneration×MF density; MF, myelinated fiber; MP, microscopic polyangitis.
The immunoreactive cell infiltrates for macrophage marker (CD68) and T cell marker (UCHL-1) were counted to assess the degree of inflammatory cell invasion in the epineurial and endoneurial areas of the nerve segments.

rophages act as scavengers of tissue degradation products and myelin debris (Marcinkiewicz et al., 1999). Macrophages bearing MRP14, a macrophage differentiation antigen associated with early active lesions (Kiefer et al., 1998), expressed more NGF mRNA in both the epineurial and endoneurial spaces of the lesioned nerves. Most of MRP14+ macrophages were round-shaped. In contrast, macrophages expressing MRP8, a macrophage differentiation antigen in chronic lesions (Kiefer et al., 1998) expressed less NGF mRNA, especially in the endoneurium. These findings suggest that NGF expressed in round-shaped and MRP14+ macrophages can be an early signal for the regeneration and repair process in vasculitic nerve lesions. NGF expression by macrophages in the endoneurium has been reported to be up-regulated by inflammatory reactions where cytokines such as IL-1β are expressed, and to lead to the establishment of a favorable environment for nerve repair and recovery (Deprez et al., 2001; Shamash et al., 2002). NGF-negative or weakly positive macrophages, most of which are MRP8+ and irregular-shaped, are thought to function in phagocytosis of myelin debris in the endoneurium, also promoting nerve regeneration (Marcinkiewicz et al., 1999). Moreover, epineurial MRP8+ macrophages harbor relatively higher levels of NGF mRNA compared with endoneurial cells, and may collaborate with T cells in an immunoregulatory cascade of vasculitic neuropathy. Epineurial NGF from MRP14+ and MRP8+ macrophages may play an instrumental role in the perivascular inflammatory circuit, or alternatively may direct the repair of injured axons through the damaged permeable perineurium (Sugimoto et al., 2002).

In addition to macrophages, infiltrating T cells also expressed NGF mRNA, regardless of whether their surface markers identified them as helper CD4+, suppressor CD8+, or activating CD3+. The expression pattern of NGF mRNA in T cells was different from that in macrophages: in macrophages, the level of NGF mRNA was heterogeneous depending on the cell shape and surface markers, but T cells in the endoneurium expressed NGF mRNA regardless of the T cell markers. It has been demonstrated previously that activated T cells produce NGF in lesions of the injured CNS or PNS to enhance nerve repair (Santambrogio et al., 1994; Moalem et al., 2000). The present study showed that T cells infiltrating the endoneurial space appear to be authorized to express NGF in. NGF

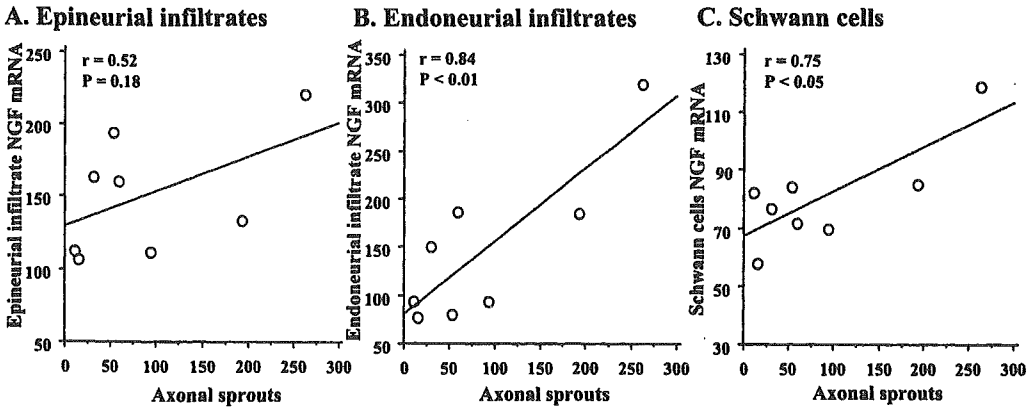

Fig. 5. Relationship between nerve regeneration and NGF mRNA expression in the epineurial and endoneurial spaces. The intensity of NGF mRNA signals was quantified as described in the text, and was expressed as signal intensity per square millimeter for the epineurial and endoneurial infiltrates and Schwann cells in each patient. Simple correlation analysis was performed between regional NGF mRNA expression and axonal regenerating sprouts.

expressed in T cells in the epineurial perivascular lesions plays a secondary role to generate inflammation that may then function to bias toward a Th2 environment, which helps the interstitial reaction and subsequent recovery from a pathological condition (Santambrogio et al., 1994). T cells are obviously involved in the complex mechanism of formation and recovery of inflammatory pathology. NGF itself reportedly promotes differentiation of T cells (Matsuda et al., 1988; Ehrhard et al., 1993). NGF mRNA expression in CD4+ and CD8+ cells in the epineurial and endoneurial spaces may suggest that such up-regulation of NGF mRNA is one aspect of the complex network of events constituting nerve regeneration and repair.

Schwann cells are another NGF producer, as shown in the present study. NGF mRNA expression in Schwann cells was up-regulated and occurred diffusely in the endoneurium of the vasculitic lesions, suggesting that lesion-induced expression of NGF occurs in Schwann cells. In the endoneurium of the lesioned nerves, NGF is produced abundantly by Schwann cells as well as MRP14+ macrophages, and acts as a neurotrophic signal to promote axonal regeneration with TrkA in sensory axons. This putative cascade was supported by the present finding that NGF mRNA expression in Schwann cells was closely correlated with the degree of axonal regeneration sprouts.

Nerve injury by axotomy, in which axonal pathology with Wallerian degeneration is the major pathological process, is considered to be an analogous animal model of the endoneurial lesions in acute vasculitic neuropathies in human (Ito et al., 1998). In the axotomy model, IL-1β and IL-6 mRNAs rapidly increase after nerve damage, while NGF mRNA shows a two-peaked increase in the early and late phases (Ito et al., 1998). The early and late peaks of NGF mRNA expression are thought to occur in round-shaped epineurial hematogenous macrophages and Schwann cells, respectively. In human acute necrotizing vasculitic neuropathies in the present study, the nerve tissues were mostly obtained within 1 week after the onset of neuropathy. Pathological findings in the endoneurial space seem to correspond to the late phase of axotomized nerves in animals. This notion agrees with the findings that endoneurial NGF mRNA was mainly derived from Schwann cells as well as MRP14+ macrophages. As demonstrated here, MRP14+ early macrophages were also present concomitantly with MRP8+ late macrophages in the endoneurium of biopsied specimens. In addition to Schwann cells and macrophages, endoneurial fibroblasts may be another cellular source of NGF in the endoneurium of injured nerves as reported previously (Marcinkiewicz et al., 1999), since NGF mRNA signals was not completely consistent with the cellular markers for Schwann cells and macrophages.

We demonstrated that NGF mRNA expression in the infiltrating cells and Schwann cells showed a good correlation with the extent of axonal sprouts of regeneration but not with that of axonal degeneration. This finding is well consistent with our previous finding using multivariate analysis that NGF mRNA levels were not related to the extent of axonal degeneration (Yamamoto et al., 2001; Sobue et al., 1998). NGF is known to induce axonal collateral sprouting in cell culture (Gallo and Letourneau, 1998; Itoh et al., 1998). Axonal regeneration is likely associated with NGF mRNA expression in the endoneurium mainly derived from MRP14+ macrophages as well as Schwann cells, and both types of cells collaborate in denervated nerves (Tofaris et al., 2002). The extent of axonal regeneration was very slight in the acute phase of vasculitic neuropathies, particularly as compared with the extent in chronic axonal neuropathy such as Charcot-Marie-Tooth disease type X (Hattori et al., 2003), showing abundant axonal sprouts. Direct evidence that activated macrophages are present at the sprouting sites was not found in this study, since the lesions caused by human vasculitic neuropathies are temporally and spatially multifocal and dispersive, not synchronous (Batchelor et al., 2002). As a correlation between the degree of axonal regeneration and the number of infiltrated macrophages is not significant in the present data, it is likely that NGF itself enhances axonal regeneration in nerve lesions of vasculitic neuropathies. Moreover, other neurotrophic factors such as brain-derived neurotrophic factor and neurotrophin-3 may be involved in axonal regeneration, since their mRNA expression levels were correlated with the extent of macrophage invasion in injured human nerves as reported in our previous studies (Sobue et al., 1998; Yamamoto et al., 1998b; Ito et al., 2001). Further studies whether axonal regenerating sprouts are the neuritis of peptidergic DRG neurons with TrkA will be needed.

Taken together, our findings on the double labeling of NGF mRNA and cellular markers clearly demonstrated that early-activated macrophages and Schwann cells are the major source of NGF expression in human nerve lesions of acute necrotizing vasculitic neuropathies, providing a clue about axonal regeneration and nerve repair. Targeted modulation of hematogenous macrophage NGF will help to promote nerve regeneration for the treatment of acute vasculitic neuropathies (Heuss et al., 2000). Further investigations will be required to determine how macrophage NGF, with the cytokine network, operates differentially in the epineurial and endoneurial areas for the recovery of vasculitic neuropathies.

Acknowledgments—This work was supported by a grant for COE (Center of Excellence) Research from the Ministry of Education, Science and Culture of Japan, and grants from the Ministry of Health, Labor and Welfare of Japan.

REFERENCES

Apfel SC, Arezzo JC, Lipson L, Kessler JA (1992) Nerve growth factor prevents experimental cisplatin neuropathy. Ann Neurol 31:76–80.

Batchelor PE, Porritt MJ, Martinello P, Parish CL, Liberatore GT, Donnan GA, Howells DW (2002) Macrophages and microglia produce local trophic gradients that stimulate axonal sprouting toward but not beyond the wound edge. Mol Cell Neurosci 21:436–453.

Brown MC, Perry VH, Lunn ER, Gordon S, Heumann R (1991) Macrophage dependence of peripheral sensory nerve regeneration: possible involvement of nerve growth factor. Neuron 6:359–370.

Chao MV, Hempstead BL (1995) p75 And Trk: a two-receptor system. Trends Neurosci 18:321–326.

Cosgaya JM, Chan JR, Shooter EM (2002) The neurotrophin receptor p75NTR as a positive modulator of myelination. Science 298:1245–1248.

Deprez M, Lubke U, Verlaet M, Debrus S, Delvenne P, Martin JJ (2001) Detection of cytokines in human sural nerve biopsies: an immunohistochemical and molecular study. Acta Neuropathol (Berl) 101:393–404.

Ehrhard PB, Erb P, Graumann U, Otten U (1993) Expression of nerve growth factor and nerve growth factor receptor tyrosine kinase Trk in activated CD4-positive T-cell clones. Proc Natl Acad Sci USA 90:10984–10988.

Fischer SJ, Podratz JL, Windebank AJ (2001) Nerve growth factor rescue of cisplatin neurotoxicity is mediated through the high affinity receptor: studies in PC12 cells and p75 null mouse dorsal root ganglia. Neurosci Lett 308:1–4.

Gallo G, Letourneau PC (1998) Localized sources of neurotrophins initiate axon collateral sprouting. J Neurosci 18:5403–5414.

Greeson DM, Moix L, Meier M, Armstrong DM, Wiley RG (1992) A continuing signal maintains NGF receptor expression in hypoglossal motor neurons after crush injury. Brain Res 594:351–355.

Hantzopoulous PA, Suri C, Glass DG (1994) The low affinity NGF receptor, p75, can collaborate with each of the Trks to potentiate functional responses to the neurotrophins. Neuron 13:187–201.

Hattori N, Ichimura M, Nagamatsu N, Li M, Yamamoto K, Kumazawa K, Mitsuma T, Sobue G (1999) Clinicopathological features of Churg-Strauss syndrome-associated neuropathy. Brain 122:427–439.

Hattori N, Yamamoto M, Yoshihara T, Koike H, Nakagawa M, Yoshikawa H, Ohnishi A, Hayasaka K, Onodera O, Baba M, Yasuda H, Saito T, Nakashima K, Kira J, Kaji R, Oka N, Sobue G (2003) Demyelinating and axonal features of Charcot-Marie-Tooth disease with mutations of myelin-related proteins (PMP22, MPZ and Cx32): a clinicopathological study of 205 Japanese patients. Brain 126:134–151.

Hawke SH, Davies LRP, Guo YP, Pollard JD, McLeod JG (1991) Vasculitic neuropathy: a clinical and pathological study. Brain 114:2175–2190.

Hayakawa K, Itoh T, Niwa H, Mutoh T, Sobue G (1998) NGF prevention of neurotoxicity induced by cisplatin, vincristine and taxol depends on toxicity of each drug and NGF treatment schedule: in vitro study of adult rat sympathetic ganglion explants. Brain Res 794:313–319.

Heumann R, Lindholm D, Bandtlow C, Meyer M, Radeke MJ, Misko TP, Shooter E, Thoenen H (1987) Differential regulation of mRNA encoding nerve growth factor and its receptor in rat sciatic nerve during development, degeneration, and regeneration: role of macrophages. Proc Natl Acad Sci USA 84:8735–8739.

Heuss D, Probst-Cousin S, Kayser C, Neundorfer B (2000) Cell death in vasculitic neuropathy. Muscle Nerve 23:999–1004.

Ito Y, Yamamoto M, Li M, Doyu M, Tanaka F, Mutoh T, Mitsuma T, Sobue G (1998) Differential temporal expression of mRNAs for ciliary neurotrophic factor (CNTF), leukemia inhibitory factor (LIF), interleukin-6 (IL-6), and their receptors (CNTFRα, LIFRβ, IL-6Rα and gp130) in injured peripheral nerves. Brain Res 793:321–327.

Ito Y, Yamamoto M, Mitsuma T, Li M, Hattori N, Sobue G (2001) Expression of mRNAs for ciliary neurotrophic factor (CNTF), leukemia inhibitory factor (LIF), interleukin-6 (IL-6), and their receptors (CNTFRα, LIFRβ, IL-6Rα and gp130) in human peripheral neuropathies. Neurochem Res 26:51–58.

Itoh T, Niwa H, Nagamatsu M, Mitsuma T, Miyakawa A, Pleasure D, Sobue G (1998) Nerve growth factor maintains regulation of intracellular calcium in neonatal sympathetic neurons but not in mature or aged neurons. Neuroscience 82:641–651.

Jennette JC, Falk RJ, Andrassy K (1994) Nomenclature of systemic vasculitides: proposal of an international consensus conference. Arthr Rheumat 37:187–192.

Kiefer R, Kieseier BC, Bruck W, Hartung HP, Toyka KV (1998) Macrophage differentiation antigens in acute and chronic autoimmune polyneuropathies. Brain 121:469–479.

Koike H, Mori K, Misu K, Hattori N, Ito H, Hirayama M, Sobue G (2001) Painful alcoholic polyneuropathy with predominant small-fiber loss and normal thiamine status. Neurology 56:1727–1732.

Levi-Montalcini R, Skaper SD, Dal Toso R, Petrelli L, Leon A (1996) Nerve growth factor: from neurotrophin to neurokine. Trends Neurosci 19:514–520.

Luk HW, Noble LJ, Werb Z (2003) Macrophages contribute to the maintenance of stable regenerating neurites following peripheral nerve injury. J Neurosci Res 73:644–658.

Marcinkiewicz M, Marcinkiewicz J, Chen A, Leclaire F, Chretien M, Richardson P (1999) Nerve growth factor and proprotein convertases furin and PC7 in transected sciatic nerves and in nerve segments cultured in conditioned media: their presence in Schwann cells, macrophages, and smooth muscle cells. J Comp Neurol 403:471–485.

Matsuda H, Coughlin MD, Bienenstock J, Denburg JA (1988) Nerve growth factor promotes human hemopoietic colony growth and differentiation. Proc Natl Acad Sci USA 85:6508–6512.

Mitsuma N, Yamamoto M, Li M, Ito Y, Mitsuma T, Mutoh T, Takahashi M, Sobue G (1999) Expression of GDNF receptor (RET and GDNFR-α) mRNAs in the spinal cord of patients with amyotrophic lateral sclerosis. Brain Res 820:77–85.

Miyata Y, Kashihara Y, Homma S, Kuno M (1986) Effects of nerve growth factor on the survival and synaptic function of Ia sensory neurons axotomized in neonatal rats. J Neurosci 6:2012–2018.

Moalem G, Gdalyahu A, Shani Y, Otten U, Lazarovici P, Cohen IR, Schwartz M (2000) Production of neurotrophins by activated T cells: implications for neuroprotective autoimmunity. J Autoimmun 15:331–345.

Molliver DC, Wright DE, Leitner ML, Parsadanian AS, Doster K, Wen D, Yan Q, Snider WD (1997) IB4-binding DRG neurons switch from NGF to GDNF dependence in early postnatal life. Neuron 19:849–861.

Rich KM, Yip HK, Osborne PA, Schmidt RE, Johnson EM Jr (1984) Role of nerve growth factor in the adult dorsal root ganglia neuron and its response to injury. J Comp Neurol 230:110–118.

Rich KM, Luszczynski JR, Osborne PA (1987) Nerve growth factor protects adult sensory neurons from cell death and atrophy caused by nerve injury. J Neurocytol 16:261–268.

Santambrogio L, Benedetti M, Chao MV, Muzaffar R, Kulig K, Gabellini N, Hochwald G (1994) Nerve growth factor production by lymphocytes. J Immunol 153:4488–4495.

Shamash S, Reichert F, Rotshenker S (2002) The cytokine network of Wallerian degeneration: tumor necrosis factor- alpha, interleukin-1alpha, and interleukin-1beta. J Neurosci 22:3052–3060.

Snider WD, Wright DE (1996) Neurotrophins cause a new sensation. Neuron 16:229–232.

Sobue G, Yasuda T, Mitsuma T, Ross AH, Pleasure D (1988) Expression of nerve growth factor receptor in human peripheral neuropathies. Ann Neurol 24:64–72.

Sobue G, Yamamoto M, Doyu M, Li M, Yasuda T, Mitsuma T (1998) Expression of mRNAs for neurotrophic factor (NGF, BDNF and NT-3) and their receptors ($p75^{NGFR}$, trkA, trkB and trkC) in human peripheral neuropathies. Neurochem Res 23:821–829.

Sugimoto Y, Takayama S, Horiuchi Y, Toyama Y (2002) An experimental study on the perineurial window. J Periph Nerv Syst 7:104–111.

Tofaris G, Patternson P, Jessen K, Mirsky R (2002) Denervated Schwann cells attract macrophages by secretion of leukemia inhibitory factor (LIF) and monocyte chemoattractant protein-1 in a process regulated by interleukin-6 and LIF. J Neurosci 22:6696–6703.

Unger JW, Klitzsch T, Pera S, Reiter R (1998) Nerve growth factor (NGF) and diabetic neuropathy in the rat: morphological investiga-

tions of the sural nerve, dorsal root ganglion, and spinal cord. Exp Neurol 153:23–34.

Yamamoto M, Li M, Nagamatsu M, Itoh T, Mutoh T, Mitsuma T, Sobue G (1998a) Expression of low-affinity neurotrophin receptor $p75^{NTR}$ in the peripheral nervous system of human neuropathies. Acta Neuropathol (Berl) 95:597–604.

Yamamoto M, Mitsuma N, Ito Y, Hattori N, Nagamatsu M, Li M, Mitsuma T, Sobue G (1998b) Expression of GDNF and GDNFR-α mRNAs in human peripheral neuropathies. Brain Res 809:175–180.

Yamamoto M, Ito Y, Mitsuma N, Li M, Hattori N, Sobue G (2001) Pathology-related differential expression regulation of NGF, GDNF, CNTF, and IL-6 mRNAs in human vasculitic neuropathy. Muscle Nerve 24:830–833.

(Accepted 23 June 2004)
(Available online 17 September 2004)

Human Molecular Genetics, 2004, Vol. 13, No. 11 **1183–1192**
DOI: 10.1093/hmg/ddh131
Advance Access published on April 21, 2004

Sodium butyrate ameliorates phenotypic expression in a transgenic mouse model of spinal and bulbar muscular atrophy

Makoto Minamiyama, Masahisa Katsuno, Hiroaki Adachi, Masahiro Waza, Chen Sang, Yasushi Kobayashi, Fumiaki Tanaka, Manabu Doyu, Akira Inukai and Gen Sobue*

Department of Neurology, Nagoya University Graduate School of Medicine, Nagoya 466-8550, Japan

Received February 23, 2004; Revised March 24, 2004; Accepted April 5, 2004

Spinal and bulbar muscular atrophy (SBMA) is an inherited motor neuron disease caused by the expansion of a polyglutamine (polyQ) tract within the androgen receptor. Unifying mechanisms have been implicated in the pathogenesis of polyQ-dependent neurodegenerative diseases including SBMA, Huntington disease and spinocerebellar ataxias. It has been suggested that mutant protein containing polyQ inhibits histone acetyltransferase activity, resulting in transcriptional dysfunction and subsequent neuronal dysfunction. Histone deacetylase (HDAC) inhibitors alleviate neurological phenotypes in fly and mouse models of polyQ disease, although the therapeutic effect is limited by the toxicity of these compounds. We studied the therapeutic effects of sodium butyrate (SB), an HDAC inhibitor, in a transgenic mouse model of SBMA. Oral administration of SB ameliorated neurological phenotypes as well as increased acetylation of nuclear histone in neural tissues. These therapeutic effects, however, were seen only within a narrow range of SB dosage. Our results indicate that SB is a possible therapeutic agent for SBMA and other polyQ diseases, although an appropriate dose should be determined for clinical application.

INTRODUCTION

Polyglutamine (polyQ) diseases are inherited neurodegenerative disorders caused by the expansion of a trinucleotide CAG repeat in the causative genes (1,2). To date, nine polyQ diseases have been identified (3). Spinal and bulbar muscular atrophy (SBMA) is a polyQ disease affecting males, and is characterized by proximal muscle atrophy, weakness, contraction fasciculations and bulbar involvement (4–6). The number of CAG repeats in the first exon of *androgen receptor* (*AR*) gene is polymorphic with a range of 11–35 in normal population; the repeat expands to 40–62 CAGs in SBMA patients (7,8) with minimal somatic mosaicism (9). There is an inverse correlation between the CAG repeat size in *AR* and the age at onset, or the disease severity (10–12) as observed in other polyQ diseases (1). The major pathological finding of SBMA is motor neuron loss in the spinal cord and brainstem accompanied by a subclinical loss of sensory neurons in the dorsal root ganglia (5). Nuclear inclusions (NIs) containing mutant AR have been observed in the residual motor neurons and non-neuronal cells (13,14). The presence of NIs, which is a clue to the pathogenesis, is also striking in other polyQ diseases (15). These observations pointed to the cell nucleus as a crucial site of polyQ toxicity in the majority of polyQ diseases, although the exact role of NIs in the pathogenesis is yet to be elucidated (16). Our previous studies with a transgenic (Tg) mouse model of SBMA clearly demonstrated that reduction in the amount of nuclear-accumulated mutant AR results in marked improvement of SBMA phenotypes (17–19).

Numerous studies have indicated that transcriptional dysregulation is the pivotal mechanism of neuronal dysfunction in polyQ disease. Transcriptional co-activators such as cAMP-response element binding protein-binding protein (CBP) are sequestrated into the NIs through protein–protein interaction in mouse models and patients with polyQ diseases (20,21). Alternatively, the interaction between transcriptional co-activators and soluble mutant protein has also been demonstrated in fly and mouse models as well as in post-mortem tissues of Huntington disease (HD) patients (22,23). The histone acetyltransferase (HAT) activity of CBP is inhibited in a fly model of HD and restored by histone deacetylase (HDAC) inhibitors, resulting in less neurodegeneration (24,25). Oral administration of suberoylanilide hydroxamic acid

*To whom correspondence should be addressed at: Department of Neurology, Nagoya University Graduate School of Medicine, 65 Tsurumai-cho, Showa-ku, Nagoya 466-8550, Japan. Tel: +81 527442385; Fax: +81 527442384; Email: sobueg@med.nagoya-u.ac.jp

(SAHA), an HDAC inhibitor, ameliorates motor impairment in a mouse model of HD (26), but its beneficial effect is restricted by lethal toxicity. In the present study, we report that oral administration of sodium butyrate (SB) ameliorates symptomatic and histopathological phenotypes of a mouse model of SBMA through upregulation of histone acetylation in nervous tissues. Although SB is less toxic than SAHA, this compound yielded beneficial effects within a narrow therapeutic window of dosage. Our results indicate the importance of dose determination in the clinical application of HDAC inhibitors, which are a promising new therapy for polyQ disease.

RESULTS

SB improves motor impairment in SBMA mouse model within a narrow optimal dose

SB did not alter the neuromuscular phenotypes in wild-type (Wt) mice at any of the doses we tested (data not shown). Oral administration of SB markedly ameliorated muscle atrophy, body posture and footprint pattern on walking in male Tg mice at a dose of 4 g/l (Fig. 1A and B). We quantitatively assessed motor impairment by rotarod analysis and cage activity measurement, and found remarkable amelioration of motor impairment with oral SB administration in a narrow SB dose range (Figs 2 and 3A–C). SB significantly delayed the onset (at 4 and 8 g/l) and the progression (at 4 g/l) of motor deficit detected by rotarod performance (Figs 2 and 3C). SB also elongated the period during which each motor activity declines to 50% of its maximal value (Fig. 3B). SB did not produce a substantial improvement in such motor performance at 2 g/l (Figs 2 and 3A–C). It should be noted that 16 g/l of SB accelerated the onset by ~2 weeks (Figs 2 and 3C). The number of days for 50% impairment of rotarod and cage activity were not changed with 2 and 8 g/l, but even worsened with 16 g/l (Fig. 3B). Tg mice treated with 16 g/l of SB showed swelling of the kidneys (data not shown), which was also obvious in Wt mice treated with a higher dose, 40 g/l, of SB.

Assessment of survival rate also demonstrated a similar pattern of dose-dependent response to that of motor performance. SB significantly improved the survival rate (4 g/l, $P < 0.0001$; 8 g/l, $P = 0.004$) and time to 50% survival at the dose of 4 and 8 g/l (Figs 2 and 3B), whereas 2 g/l doses of SB did not alter the survival rate (Figs 2 and 3B). On the other hand, the lifespan of Tg mice was shortened at the dose of 16 g/l (Fig. 2, $P = 0.0009$). SB treatment at 4 g/l resulted in body weight gain, whereas Tg mice given other doses of SB showed earlier declines in weight, as did those not treated with SB (Fig. 2).

These observations indicate that oral administration of SB improves motor impairment, survival rate and failure of weight gain in the male Tg mice within a narrow dose range. Nevertheless, a higher dose of SB has deleterious effects on the neurological phenotypes of Tg mice.

SB ameliorates histopathological impairments of motor neurons and muscles

Oral administration of SB at the dose of 4 g/l significantly improved histopathological impairments in the muscles, spinal motor neurons and their axons in the male Tg mice (Fig. 4). The SBMA Tg mice show atrophy of spinal motor neurons and their axons in the ventral nerve root accompanied by neurogenic amyotrophy (17). SB administration significantly increased the diameter of muscles, spinal roots and motor neurons as compared with non-treated mice. Although small angulated fibers and grouped atrophy were observed in the muscles of the non-treated group, SB markedly ameliorated these histopathological appearances of denervation pattern (Fig. 4A–C). SB also improved axonal atrophy in the L5 ventral nerve root (Fig. 4D–F). There was a significant difference in the size of large motor neurons in the lumbar

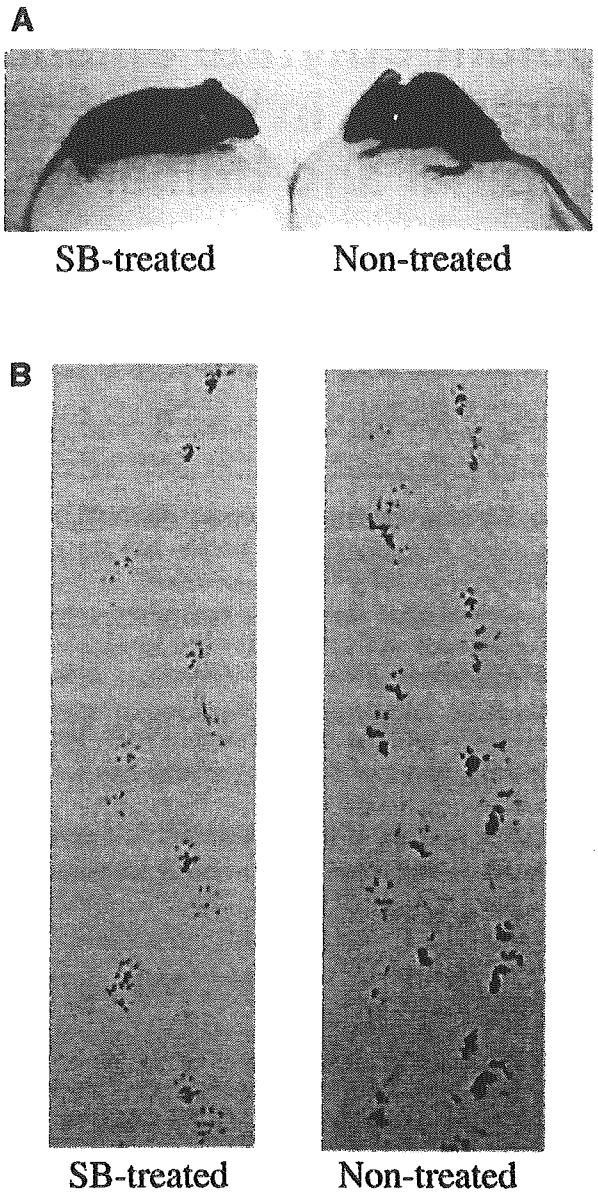

Figure 1. SB ameliorates neuromuscular phenotypes of SBMA Tg mouse. (**A**) The male Tg mouse treated with 4 g/l of SB does not show the muscular atrophy seen in the non-treated male mouse (12 weeks old). (**B**) Footprints of the SB-treated and non-treated male Tg mice. Front paws are in red, and hind paws in blue. SB markedly ameliorated gait disturbance.